Deep-Sea Research II 101 (2014) 63–79

Contents lists available at ScienceDirect

Deep-Sea Research II

journal homepage: www.elsevier.com/locate/dsr2

Boundary influences on HAB phytoplankton ecology in a stratification-enhanced upwelling shadow

J.P. Ryan [a,*], M.A. McManus [b], R.M. Kudela [c], M. Lara Artigas [d], J.G. Bellingham [a], F.P. Chavez [a], G. Doucette [e], D. Foley [f], M. Godin [a], J.B.J. Harvey [a], R. Marin III [a], M. Messié [a], C. Mikulski [e], T. Pennington [a], F. Py [a], K. Rajan [a], I. Shulman [g], Z. Wang [e], Y. Zhang [a]

[a] Monterey Bay Aquarium Research Institute, 7700 Sandholdt Road, Moss Landing, CA 95039, United States
[b] University of Hawaii at Manoa, Department of Oceanography, 1000 Pope Road Honolulu, Hawaii 96822, United States
[c] University of California, Santa Cruz, 1156 High Street, Santa Cruz, CA 95064, United States
[d] Institut de Ciències del Mar-CSIC, Barcelona, Passeig Marítim de la Barceloneta, 37-49, E-08003 Barcelona, Spain
[e] NOAA/National Ocean Service, 219 Fort Johnson Rd., Charleston, SC 29412, United States
[f] NOAA Southwest Fisheries Science Center, 1352 Lighthouse Avenue, Pacific Grove, CA 93950, United States
[g] Naval Research Laboratory, Oceanography Division, Stennis Space Center, MS 39529-5004, United States

ARTICLE INFO

Available online 21 January 2013

Keywords:
Algal blooms
Coastal oceanography
Coastal upwelling
Molecular biology

ABSTRACT

Coastal marine ecosystems are profoundly influenced by processes that originate from their boundaries. These include fluid boundaries—with the atmosphere, oceanic boundary currents and terrestrial aquatic systems, as well as solid boundaries—with the seafloor and coast. Phytoplankton populations transfer complexly interacting boundary influences into the biosphere. In this contribution, we apply data from an ocean observing and modeling system to examine boundary influences driving phytoplankton ecology in Monterey Bay, CA, USA. The study was focused on species that may cause harmful algal blooms (HABs). During September–October 2010, autonomous molecular analytical devices were moored at two locations characterized by different degrees of stratification and exposure to upwelling dynamics. The time-series revealed multiple transitions in local HAB phytoplankton communities, involving diatoms (*Pseudo-nitzschia* spp.), dinoflagellates (*Alexandrium catenella*), and raphidophytes (*Heterosigma akashiwo*). Observational and model results showed that the biological transitions were closely related to environmental changes that resulted from a variety of boundary processes—responses of oceanic circulation to wind forcing, influxes of different water types that originated outside the bay, and emergence of strongly stratified nearshore water into the greater bay. Boundary processes were further implicated at patch scales. High-resolution mapping and sampling of a phytoplankton-enriched patch were conducted in a Lagrangian framework using autonomous underwater vehicles. These highly resolved measurements showed that small-scale spatial patterns in the toxicity of *Pseudo-nitzschia* populations were related to the coupling of resuspended sediments from the bottom boundary layer to the surface mixed layer.

1. Introduction

Mitigating HAB threats to ecosystem, human, and economic health requires advancing understanding of the processes underlying bloom formation. The methods required to advance understanding depend upon the characteristics of the HAB-susceptible environment and the ecology of HAB species. One type of environment targeted for focus by the Global Ecology and Oceanography of Harmful Algal Blooms (GEOHAB) program has been termed "Stratified Systems" (GEOHAB, 2008). The GEOHAB Core Research Project on Stratified Systems emphasizes the importance of small-scale hydrographic features to HAB ecology. These hydrographic features—which can be found in upwelling systems, fjords, coastal embayments and eutrophic systems—involve large changes in stratification occurring over small spatial scales. Spatial variation in stratification, in turn, strongly influences the patterns and processes of phytoplankton ecology.

Coastal upwelling systems experience processes that reduce vertical density stratification. Strong wind forcing can reduce stratification directly, via coastal upwelling and turbulent vertical mixing, as well as indirectly, via advection of upwelled water in which vertical density stratification is weak. Coastal upwelling systems also contain environments in which geomorphological influences create localized areas of enhanced stratification. These influences include

* Corresponding author. Tel.: +1 831 775 1978; fax: +1 831 775 1620.
E-mail address: ryjo@mbari.org (J.P. Ryan).

0967-0645/$ - see front matter © 2013 Elsevier Ltd. All rights reserved.
http://dx.doi.org/10.1016/j.dsr2.2013.01.017

sheltering from intense regional wind forcing by coastal mountains, sheltering from advective influx of destratified (recently upwelled) water, and enhanced residence time. All of these influences are active in the upwelling shadow of northern Monterey Bay, California (Graham and Largier, 1997). The locally enhanced residence time and local heating of this upwelling shadow are evident in average sea surface temperature (SST), which is warmest in the northeastern bay (Fig. 1a). An AUV-based climatology shows that both thermal and haline contributions to vertical density stratification increase from a minimum at the central mouth of Monterey Bay to a maximum in the northeastern reaches of the upwelling shadow (Ryan et al., 2008a). Associated with lateral gradients in stratification and water properties across the upwelling/ shadow complex are sharp changes in the plankton communities (Graham et al., 1992; Breaker and Broenkow, 1994; Harvey et al., 2012).

Along with regional patterns of stratification, the transport of different water types into Monterey Bay largely determines the environmental conditions affecting phytoplankton. The composition of Monterey Bay water depends upon the variable influx of water types that originate outside of it (Graham and Largier, 1997). These influxes are determined largely by variable wind forcing. During upwelling favorable wind forcing, relatively cold and saline oceanic conditions develop as upwelling filaments generated outside the bay (Fig. 1a) are transported into the bay (Rosenfeld et al., 1994). During relaxation/reversal of upwelling favorable winds, upper-water-column warming and freshening typically occur in the bay. This is caused by shoreward advection of offshore water originating in the California Current System (CCS), which is fresh and warm relative to recently upwelled water, and by local surface heating that occurs under reduced wind stress (Rosenfeld et al., 1994; Graham and Largier, 1997; Ramp et al., 2005). Responses of the bay circulation to upwelling and downwelling favorable winds are often characterized by cyclonic flow (e.g. Graham and Largier, 1997; Ramp et al., 2005; Ryan et al., 2008b, 2009).

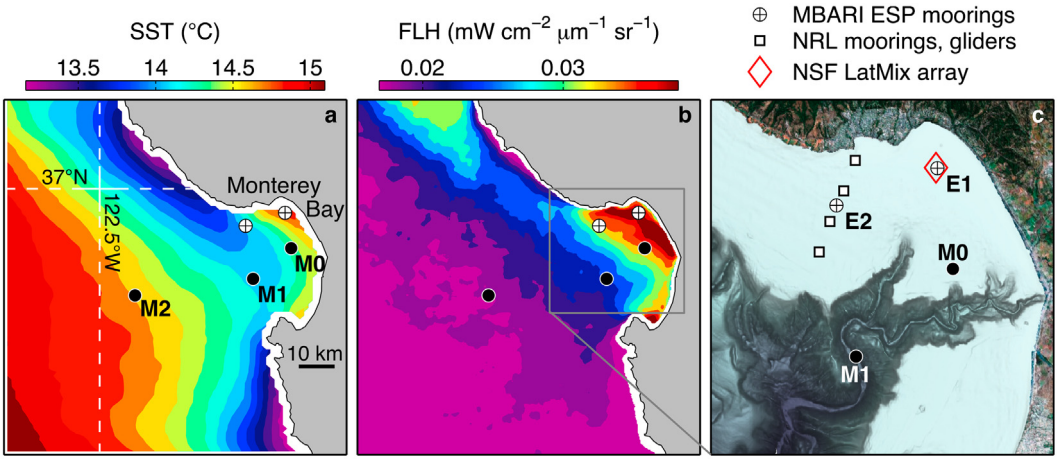

Fig. 1. Climatology-guided experiment design. Satellite-observed (a) sea surface temperature (SST) and (b) chlorophyll fluorescence line height (FLH) are means of August–November data from 2003 to 2008. Moorings M0 (70 m water depth), M1 (1200 m), and M2 (1800 m) provided regional meteorological and oceanographic data. (c) Bathymetry in the bay is shown relative to the M and ESP (E1, E2) mooring locations. ESP instruments were placed within localized observing arrays (see Materials and methods).

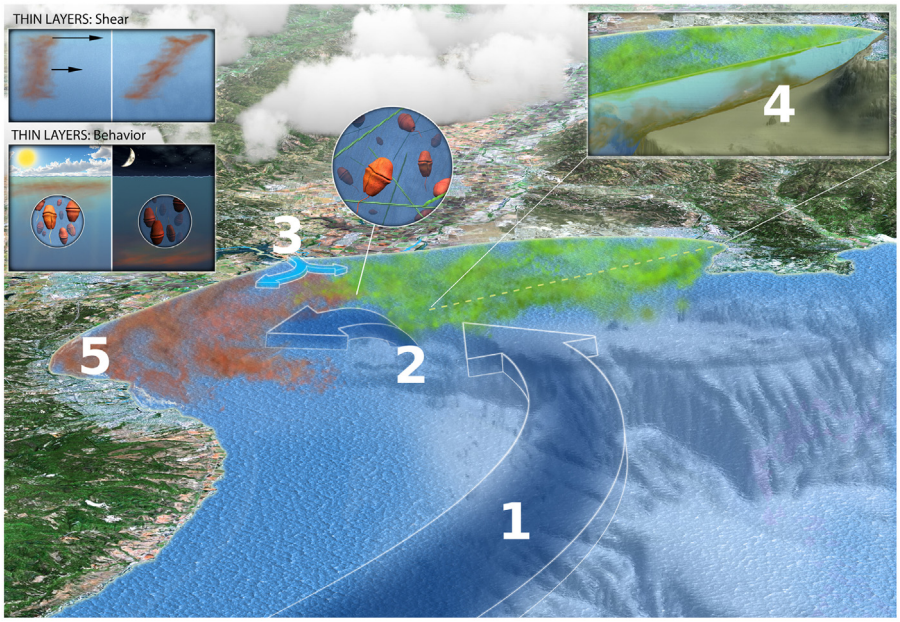

Fig. 2. A conceptual representation of boundary influences on plankton ecology in Monterey Bay. View is from the NW (Fig. 1). Numbered process indicators are described in the text.

Phytoplankton populations thrive on episodic nutrient supply within the relatively stratified water of the upwelling shadow (Fig. 1b), where blooms of various species may originate. HAB species that bloom in Monterey Bay include toxigenic diatoms of the genus *Pseudo-nitzschia* (Scholin et al., 2000; Kudela et al., 2005; McManus et al., 2008; Rienecker et al., 2008; Ryan et al., 2011), dinoflagellates including *Cochlodinium fulvescens*, *Alexandrium catenella*, and *Akashiwo sanguinea* (Curtiss et al., 2008; Kudela et al., 2008a; Ryan et al., 2008a, 2009, 2010a; Jessup et al., 2009), and the raphidophyte *Heterosigma akashiwo* (O'Halloran et al., 2006; Greenfield et al., 2008). Major differences in the composition of the HAB phytoplankton community may occur over small spatial scales within Monterey Bay. For example, during a strong upwelling pulse in October 2008, while concentrations of *Pseudo-nitzschia* spp. and the associated toxin domoic acid (DA) strongly increased in outer bay water (Ryan et al., 2011), concentrations of dinoflagellates of the genera *Prorocentrum*, *Ceratium*, *Dinophysis*, *Alexandrium*, and *Scrippsiella* increased in inner bay water (Mackey et al., 2012). Complex biological interactions also influence phytoplankton community composition in Monterey Bay. For example, the occurrence of dinoflagellate blooms and the composition of the phytoplankton community may be controlled by parasitism (Mazzillo et al., 2011).

Previous studies indicate the central importance of boundary influences to phytoplankton ecology in Monterey Bay (Fig. 2). Strong local response of toxigenic *Pseudo-nitzschia* spp. to incursion of wind-driven upwelling filaments (process 1) has been observed in situ, and toxicity was elevated and more variable where interaction between phytoplankton and resuspended sediments (process 4) occurred (Ryan et al., 2011). Benthic-pelagic coupling, between the turbid bottom boundary layer (BBL) and phytoplankton populations in the surface mixed layer, has been observed in northern and southern Monterey Bay, and in both cases the coupling occurred in frontal zones (Ryan et al., 2005a, 2011). One hypothesis for a causal link between sediments and toxicity involves the influences of trace metals on DA production, which have been observed in laboratory experiments (Rue and Bruland, 2001; Maldonado et al., 2002; Rhodes et al., 2006). Toxigenic response of *Pseudo-nitzschia* to urea has also been observed in laboratory studies (Howard et al., 2007; Kudela et al., 2008b, 2010), illustrating how anthropogenic sources of nitrogen (process 3) may influence HAB development and toxicity. Development of harmful dinoflagellate blooms in nearshore water of Monterey Bay (Jessup et al., 2009) has also indicated the potential role of episodic land drainage in bloom inception. Upwelling from Monterey Canyon onto the shelf (process 2) can be driven by internal tidal forcing (Shea and Broenkow, 1982) or steering of subtidal flows by canyon topography (Klinck, 1996). Canyon upwelling has been observed to support blooming of a HAB dinoflagellate species that forms thin layers by diurnal vertical migration (Ryan et al., 2010a), and it has been linked to coupling of the turbid bottom boundary layer to phytoplankton populations in the surface mixed layer (Ryan et al., 2005a). The role of coastal boundary refugia in the initiation of larger scale blooms and the retention of bloom populations (process 5) has been repeatedly observed (Ryan et al., 2005b, 2008a, 2009; Rienecker et al., 2008).

The present study is focused on forcing of phytoplankton ecology by variability in process 1 – upwelling and its inverse conditions induced by wind relaxation/reversal, process 4 – coupling of the bottom boundary layer to the surface mixed layer, and process 5 – circulation patterns that determine the role of refugia in seeding and retaining bloom populations. Additionally, we examine the development of blooms of vertically migratory phytoplankton populations (Fig. 2, inset) that incubated at and spread from the coastal boundary.

2. Materials and methods

The GEOHAB Core Research Project on Stratified Systems emphasizes the need for application of novel methods to understand the complex relationships between aquatic ecosystem processes and HAB dynamics. In this research we employed multiple emergent methods integrated with more traditional methods to resolve HAB ecological processes.

2.1. Autonomous molecular detection of HAB species and toxin

A key capability for this study was provided by the Environmental Sample Processor (ESP), which enables autonomous in situ detection of HAB phytoplankton species and the toxin domoic acid (DA) (Greenfield et al., 2008; Scholin et al., 2009; Doucette et al., 2009). Although ESP can target bacteria (Preston et al., 2011) and zooplankton (Harvey et al., 2012), all ESP sampling capacity in the present study was devoted to HAB detection. The deployed ESP arrays permitted quantifying abundances of *Pseudo-nitzschia australis*, *Pseudo-nitzschia multiseries*, combined signal from *P. multiseries* and *Pseudo-nitzschia pseudodelicatissima*, *H. akashiwo*, *A. catenella*, and concentrations of particulate DA (pDA). Although limited, the phytoplankton probe set spans the major HAB phytoplankton groups found in coastal upwelling systems (Trainer et al., 2010). ESP methods for sampling and quantification of HAB species and pDA, environmental sensors deployed with each ESP, and data telemetry have been described elsewhere (Greenfield et al., 2008; Scholin et al., 2009; Doucette et al., 2009); these methods are not described here.

ESP deployment locations were chosen relative to average conditions derived from satellite data (Fig. 1), as well as coordination with two research programs aimed at physical and optical oceanographic studies of Monterey Bay: (1) the Lateral Mixing project supported by the National Science Foundation and (2) the BIO-optical Studies of Predictability and Assimilation in the Coastal Environment (BIOSPACE) project, supported by the Naval Research Laboratory. Site E1 was located within the warmest, most chlorophyll-rich water of northern Monterey Bay (36.9325°N, 121.9225°W; water column depth 20 m; mean sample depth 7.4 m). Site E2 was located toward the outer boundary of the upwelling shadow, where direct encounter with upwelling filaments was more probable (36.8958°N, 122.0458°W; water column depth 50 m; mean sample depth 6.2 m). For consistent sampling within the diurnal cycle, ESP sampling was scheduled for the same time of a day, 9 am, and sampling between the two sites was synchronized. Sampling for DA followed sampling for HAB species by 2–3 h. Measurements by environmental sensors deployed alongside ESPs were acquired every 5 min, at higher frequency than in previous deployments, to better resolve rapid changes associated with the passage of internal waves (e.g. Ryan et al., 2011).

2.2. Autonomous underwater vehicle (AUV) surveys

AUVs provided another key capability for advancing HAB ecological studies in this experiment. Propelled AUVs, which excel at providing synoptic multidisciplinary observations, have been applied to study a variety of complex coastal ocean processes in the Monterey Bay region (Fitzwater et al., 2003; Ryan et al., 2005a, 2008a, 2008b, 2009, 2010a, 2010b, 2010c, 2011; Johnson and Needoba, 2008; Cazenave et al., 2011; Harvey et al., 2012). In the first series of ESP network experiments (2007–2008), data from AUVs provided detailed information about environmental and biological patchiness, enabling characterization of processes driving variability in HAB species and DA (Ryan et al., 2011). While these observations supported important

insights, they also clearly revealed methodological improvements required to effectively study patchy HAB phytoplankton populations. One such improvement was integrated recognition, localization, tracking, and sampling of patches. Since the earlier ESP network experiments, autonomous patch recognition and sampling have been developed and applied to studies of phytoplankton (Zhang et al., 2010) and zooplankton (Ryan et al., 2010b), and autonomous tracking capabilities for individual and coordinated AUVs have been developed and applied (Godin et al., 2011; Das et al., 2012). These capabilities were deployed on two AUVs in this experiment.

The AUV *Dorado* and its *Gulper* water-sampling system have been described elsewhere (Bellingham et al., 2000; Ryan et al., 2010b). The phytoplankton patch-sampling algorithm implemented on *Dorado* integrates multiple capabilities (Zhang et al., 2010). It (1) accumulates statistics of profile-peak and background magnitudes of chlorophyll fluorescence and optical backscattering within a temporal window, thereby adapting sensitivity to ambient conditions, (2) targets sampling at coincident peaks in fluorometric chlorophyll and optical backscattering, to ensure that sampled fluorescence peaks are true biomass maxima and not false subsurface peaks due to quenching of fluorescence near the surface (Cullen and Eppley, 1981; Holm-Hansen et al., 2000), and (3) allocates AUV sampling capacity throughout a survey. *Dorado* was operated in two modes, one for patch localization and the other for patch tracking. Both survey types involved sampling a volume, however, the first was organized in a Eulerian frame of reference whereas the second was organized in a Lagrangian frame of reference. The Lagrangian survey presented here involved coordinated operations with a second AUV, *Tethys*, as described below.

Also known as the long-range AUV (Bellingham et al., 2010), *Tethys* is capable of more sustained operations. Whereas *Dorado* operations required deployment and recovery on a daily cycle, *Tethys* was deployed for missions of up to 5 days during this experiment. Tethys conducted exploratory surveillance to localize a phytoplankton-enriched patch in the same area as *Dorado* large-scale volume surveys. The profile-based peak-detection algorithm operating on *Dorado* (Zhang et al., 2010) was also used on *Tethys*. The vertical localization signal from this algorithm was in turn used for horizontal localization of the patch center while *Tethys* executed a search algorithm. This algorithm was designed to provide the high temporal resolution required to address the challenge of a rapidly changing environment (Godin et al., 2011). Following coordinated localization of a phytoplankton-enriched patch, the AUVs cooperated to map and sample the evolving patch in a Lagrangian framework. The patch was tagged by a satellite-tracked drifter, which had a 1 m^3 drogue at ~10 m depth, and it was tracked for a distance of ~20 km over ~2 days. *Tethys* autonomously tracked the drifter and continued to execute volume surveys, providing data to determine the spatial offset between the drifter location and an estimate of the true patch centroid computed from fluorometric chlorophyll data (Godin et al., 2011). The optimized patch centroid information was relayed to *Dorado*, which utilized periodically updated positions to conduct volume surveying and targeted sample acquisition within the patch. Sample acquisition was accomplished with the *Gulper* water sampling system, composed of 10 independently controlled 1.8 L sample containers that rapidly fill (1–2 s) to acquire samples from specific features (Bird et al., 2007; Ryan et al., 2010b).

In addition to propelled AUVs, we used a Slocum glider to provide a time-series of vertical sections parallel to and ~1 km west of the NRL mooring array and E2 (Fig. 1c). Details of this glider and its sensors are published (Penta, 2011). To illustrate the hydrographic transition associated with a transition in the HAB community at E2, we present glider sections of temperature, salinity and fluorometric chlorophyll.

2.3. AUV water sample processing

We present two results from AUV-acquired water samples: (1) enumeration of toxigenic diatoms of the genus *Pseudo-nitzschia* and (2) measurements of particulate domoic acid. For phytoplankton enumeration, 50 mL aliquots were fixed with glutaraldehyde at a concentration of 2%. Black PC Nucleopore filters of 25 mm diameter and 0.2 μm pore size were used to retain organisms contained in 10 mL of sample. Filters were mounted on a glass slide with immersion oil and frozen at −80 °C until enumeration. Samples were defrosted and the entire slide was examined under epifluorescence microscopy. DAPI staining (50 μL of DAPI per filter) was selectively applied to aid identification of small organisms in some of the AUV samples, only when the method would clearly be beneficial, not routinely. When *Pseudo-nitzschia* were of low to moderate abundance, enumeration included the entire plate. When *Pseudo-nitzschia* were of high abundance, enumeration included one to several transects, determined with the X-axis mechanical stage scale and the width of the field.

For measurement of pDA, approximately 900 mL of each 1.8 L water sample was vacuum filtered though a 60 μM, 25 mm nylon net filter to collect zooplankton (data not considered here). Approximately 450 mL was then filtered through a 0.65 μM, 25 mm Durapore filter (Millipore, Billerica, MA) to collect pDA. Filters were immediately placed in 2 mL cryovials and stored in liquid nitrogen prior to overnight shipping on dry ice from MBARI to the NOAA Charleston laboratory, where they were stored at −80 °C until DA extraction and analysis. Filters were extracted using 10% aqueous methanol and analyzed for DA by liquid chromatography-tandem mass spectrometry (Wang et al., 2012). An HP1100 binary LC system (Agilent Technologies, Palo Alto, CA, USA) coupled to an AB Sciex API 4000 triple quadrupole mass spectrometer equipped with a Turbo V™ source (AB Sciex, Foster city, CA, USA) was used for the analyses. LC separations employed a Luna C18(2) column (150 mm × 2 mm, 5 μm; Phenomenex, Torrance, CA, USA) with a flow rate of 0.2 mL min^{-1}. The mobile phase consisted of water (A) and acetonitrile (B) in a binary system, with 0.1% formic acid as an additive. Domoic acid detection was achieved by multiple reaction monitoring (MRM) in positive ion mode. Four MRM transitions from the protonated DA ion were monitored: m/z 312→266, m/z 312→248, m/z 312→193, and m/z 312→161. Quantification was based on a certified DA reference material (CRM-DA-f; CRMP, NRC Institute for Marine Biosciences, Halifax, NS, Canada).

2.4. Moored environmental sensing

In addition to environmental measurements associated with the ESP network, environmental sensing was augmented by meteorological and oceanographic measurements at long-term mooring sites, M0, M1, and M2 (Fig. 1). In this study we examined wind forcing and oceanographic responses using wind observations from all M moorings and water column measurements of temperature and salinity at M1 and M0. Details of the M-mooring sensors have been described elsewhere (Ryan et al., 2011). Full-water column measurements were provided by a *SeaHorse* autonomous moored vertical profiler, as part of the NSF-funded "Lateral mixing and dispersion on the inner shelf" (LatMix) program that operated an observing array within which E1 was placed (Fig. 1c). The profiler was deployed 150 m west of E1. Previous studies demonstrated the effectiveness of the *SeaHorse* profiler for studies of phytoplankton thin-layer ecology in Monterey Bay (Ryan et al.,

2008b). High-resolution (<2 cm) vertical profiles were collected every 30 min between the bottom and the surface. SeaHorse sensors included (1) a SeaBird SBE-19+ CTD that measured temperature, conductivity (salinity), and pressure, (2) a SeaBird SBE-43 sensor that measured dissolved oxygen, and (3) a WET Labs WET Star chlorophyll fluorometer, and (4) a WET Labs cs-25-66-p (red) C-Star transmissometer that measured beam transmittance.

2.5. Sensor calibration and standards of data reporting

Adhering to the most recently adopted standards for the Thermodynamic Equation of State, we present salinity data from all platforms as absolute salinity (S_A) and use S_A in computations of density (IOC, 2010). Sensors on all platforms were independently calibrated according to manufacturer standards. Analyses of data from the Lagrangian patch tracking required intercalibration of measurements from the *Dorado* and *Tethys* AUVs, which were operating within the same domain to map a phytoplankton patch. The chlorophyll fluorometer on *Dorado* was calibrated with lab-based extractive chlorophyll measurements from samples acquired by the AUV's water sampling system. Therefore it was deemed effectively calibrated relative to in situ chlorophyll concentrations. *Tethys* fluorometric chlorophyll concentration and optical backscattering data from the same sampling domain were matched with *Dorado* data, and a least-squares fit between median profile data from both AUVs was computed. *Tethys* data were then adjusted according to this relationship.

2.6. Satellite remote sensing

To define average conditions (Fig. 1), which were in turn used to inform ESP moorings placement, we used surface chlorophyll fluorescence line height from the Moderate Resolution Imaging Spectroradiometer (MODIS) Aqua satellite sensor. True-color images from MODIS were also used to examine patterns of patchiness in highly visible dinoflagellate blooms. Processing methods for MODIS data are documented elsewhere (Ryan et al., 2009). To quantify the near-infrared reflectance signal of dinoflagellate 'red tide' blooms and examine their development, we used the Maximum Chlorophyll Index (MCI) from the Medium Resolution Imaging Spectrometer (MERIS) (Gower et al., 2005; Ryan et al., 2008a, 2009). To examine regional sea surface temperature (SST) patterns, we used data from the Advanced Very High Resolution Radiometer (AVHRR) constellation of sensors, which provide greater temporal resolution than MODIS. AVHRR processing methods are documented elsewhere (Ryan et al., 2010c). To augment observations of phytoplankton patchiness, we tasked two instruments on the ALOS satellite with opportunistic observation: (1) the Advanced Visible and Near-Infrared Radiometer, type 2 (AVNIR-2), which provides color images at 10 m resolution, and (2) the Panchromatic Remote-sensing Instrument for Stereo Mapping (PRISM), which provides 2.5 m resolution images at nadir in the spectral band 520 to 770 nm. On 12 October 2010, these sensors provided simultaneous imaging of Monterey Bay.

2.7. Event response sampling

Targeted mapping of near-surface properties and sampling of phytoplankton were conducted occasionally using the *R/V John Martin*. In this study we present results from a single event-response survey motivated by satellite remote sensing observations of a bloom patch that was emerging from a near-coastal refuge and influencing one of the ESP sites. Samples, collected using the vessel underway mapping system (intake $\sim$2 m depth), were targeted according to real-time examination of fluorometric chlorophyll data. Samples were placed in 25 mL glass bottles and kept in dark and cold until being fixed and processed upon arrival in the laboratory, in the afternoon of the sampling day. Microscopy methods were as described in Section 2.3. Focusing on the dominant phytoplankton in the dense bloom patch, we enumerated only the most abundant phytoplankton along one central transect of each slide.

2.8. Modeling of the origins and transport pathways of water masses

To investigate the origins of water contributing to hydrographic and biological transitions at the ESP sites, we used a modeling approach previously applied to study the distributions of bioluminenscence mapped by AUVs in coastal water. The approach is based on using an adjoint to the passive tracer with velocities and diffusivities derived from a circulation model (Shulman et al., 2010, 2011). The Monterey Bay circulation model is based on the Navy Coastal Ocean Model (NCOM), which is a primitive-equation, 3D, hydrostatic model. It uses the Mellor–Yamada level 2.5 turbulence closure scheme and the Smagorinsky formulation for horizontal mixing. The model is forced with surface fluxes from the Coupled Ocean and Atmospheric Mesoscale Prediction System (COAMPS) (Doyle et al., 2009) at 3 km horizontal resolution. The Monterey Bay model uses the Navy Coupled Ocean Data Assimilation (NCODA) system (Shulman et al., 2011). The NCODA assimilates satellite altimeter observations, satellite sea surface temperature, as well as available in situ vertical temperature and salinity profiles from ships and gliders. The adjoint passive tracer analysis quantifies spatially dependent contributions of tracer-tagged water that was advected and mixed into a target volume over a specified period preceding a specified seed time. In this study, the target areas were defined as volumes around the ESP moorings (4×4 km horizontal, upper 20 m), the specified times of interest were the ecological transitions identified from observational data, and the period preceding the transitions was set to 3.5 days.

3. Results

3.1. Regional variability during the study

Although characteristic patterns occur in regional oceanic responses to wind forcing, as described in the Introduction, local responses to wind forcing are complicated by multivariate dependence—spatial variation in wind stress and oceanic residence times, variable 'background' circulation patterns and water-type distributions present when wind forcing changes, and variable integrated history of wind forcing, i.e. duration and intensity of prevailing winds and their transitions (Smayda and Trainer, 2010). This complexity is illustrated by the time-series of spatially varying winds and oceanic conditions (Fig. 3). Regional winds off central California, to which Monterey Bay circulation is strongly responsive, are well represented at M2 (Fig. 3a). We classify regional wind forcing regimes based on M2 winds as (1) upwelling (unshaded periods), when alongshore-equatorward winds conducive to coastal upwelling were persistent, or (2) relaxation (shaded periods), when upwelling favorable winds were relaxed or reversed (poleward) for at least 1 day (Fig. 3a). Compared to winds at M2, winds within the bay are considerably weaker (Fig. 3a–c). Although weaker, winds at the mouth of the bay (M1) exhibited the same general patterns of upwelling and relaxation as the regional winds measured at M2 (Fig. 3a,b). The duration and intensity of wind relaxation/reversal events increased throughout the experiment (Fig. 3a, shaded periods). Consistent with the increasing influence of wind relaxation/

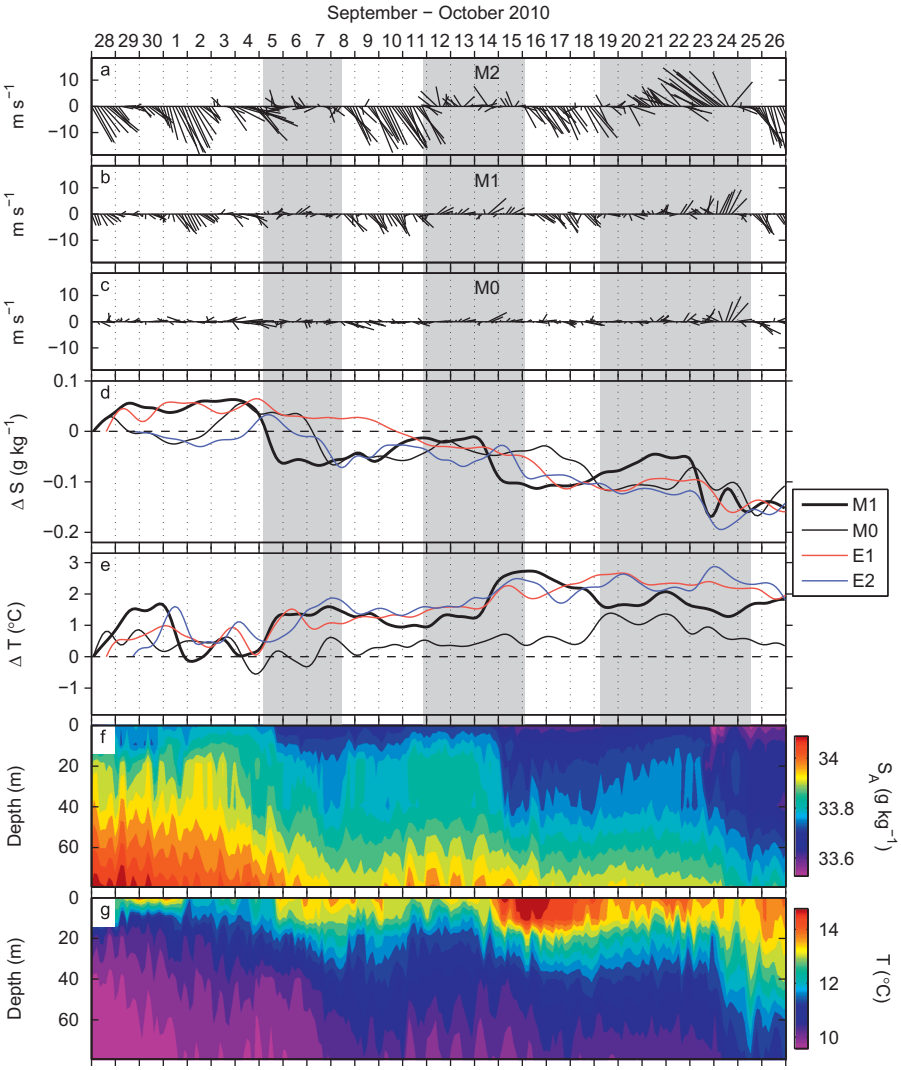

Fig. 3. Spatially variable wind forcing (a–c) and water column variability (d–g) during the experiment, based on data from the M and E moorings (Fig. 1). M2 (a) is most representative of regional wind forcing. Shaded periods indicate when regional winds were not persistently upwelling favorable (equatorward), but were instead relaxed or reversed for at least 1 day. (d,e) Cumulative changes in surface water properties at the M moorings and subsurface (~7 m) at the E moorings, 33-h low-pass filtered. (f,g) Water column salinity and temperature at M1. Time is PDT.

reversal during the study, all mooring locations showed net increases in surface temperature and decreases in surface salinity (Fig. 3d,e). The salinity variations were driven by oceanic transport patterns, rather than precipitation and land drainage. Water column observations at M1 further showed that the increasing intensity of wind relaxations affected a progressively greater extent of the water column (Fig. 3f,g). Although similar net changes in oceanic conditions occurred at all mooring locations, the timing, magnitude, and temporal progression of changes were quite different between locations (Fig. 3d,e).

3.2. Environmental and HAB phytoplankton variability at the ESP sites

While both ESP locations exhibited similar trends in temperature and salinity variation, E1 experienced higher levels of salinity and chlorophyll (Fig. 4a–c). Higher chlorophyll concentrations at E1 (Fig. 4c) are consistent with climatological patterns (Fig. 1b). All HAB targets and pDA were detected (Fig. 4d–i). Only pDA (Fig. 4d) exhibited significant correlation ($p < 0.05$) between the two sites. The absence of significant correlation between time-series for HAB phytoplankton illustrates small-scale variability in community composition (the sites were separated by only 11.5 km). Composition of the toxigenic *Pseudo-nitzschia* population also exhibited a clear difference between the two sites; *P. multiseries* was detected only at E2 (Fig. 4g).

Intra-site variations in the HAB community exhibited clear relationships (Fig. 4; Table 1). We consider these relationships in terms of two phytoplankton ecotypes among the deployed ESP probe set. The first are pennate diatoms of the genus *Pseudo-nitzschia*, which are often associated with relatively stronger upwelling exposure and weaker stratification (Trainer et al., 2000; Smayda and Trainer, 2010; Ryan et al., 2011) (Fig. 4e-g, probes auD1, muD2 and muD1 in Table 1). The second group is dinoflagellates and raphidophytes, which are often associated with relatively weaker upwelling exposure and stronger stratification, such as occurs spatially in sheltered water and temporally during relaxation of upwelling favorable winds (Ryan et al., 2008a; Bravo et al., 2010; Smayda and Trainer, 2010) (Fig. 4h,i; probes Het and NA1 in Table 1). While these generalizations about ecotypes may apply in many environments, it is important to recognize that some dinoflagellates, including *Alexandrium*, are well adapted to the dynamic conditions of coastal upwelling systems (Smayda, 2010; Kudela et al., 2010). In our time-series, significant ($p < 0.05$)

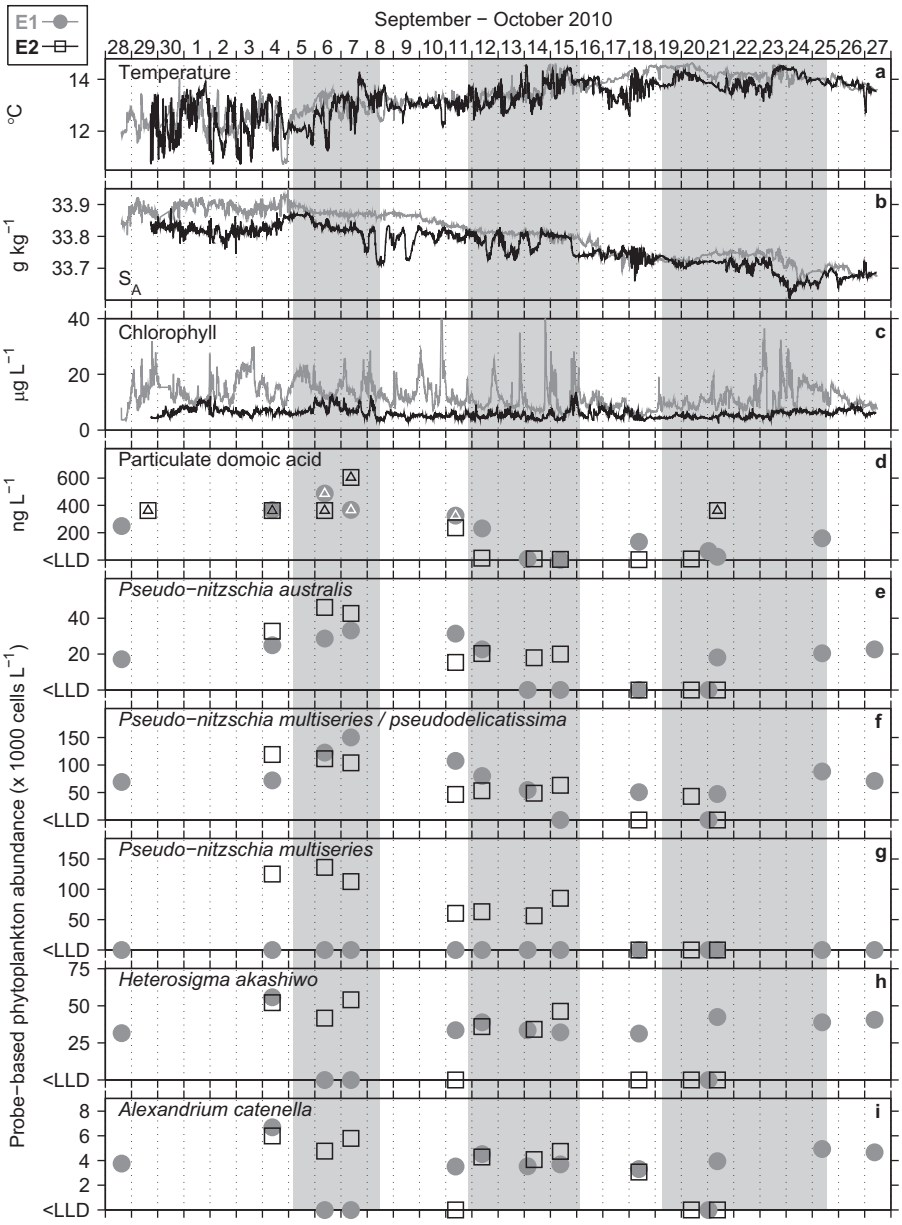

Fig. 4. ESP system measurements at both locations (Fig. 1c), including environmental data at 5-minute resolution (a–c) and HAB molecular detection results (d–i). Results from E1 (E2) are shown in gray (black) lines and symbols (legend in upper left). LLD indicates the lower limit of detection for the ESP molecular probes. pDA symbols containing triangles indicate that the assay sensitivity was surpassed and thus actual concentrations exceeded the value shown. Shaded periods correspond with regional wind relaxation/reversal (as in Fig. 3). Time is PDT.

covariation occurred between HAB phytoplankton of the same ecotype, and no significant covariation occurred between HAB phytoplankton of different ecotypes (Table 1). Exhibiting higher levels of *Pseudo-nitzschia* spp. and pDA during approximately the first half of the experiment (Fig. 4d–g), time-series at both sites indicate general covariation between these toxin producers and particulate concentrations of their toxin. However, these relationships were statistically significant only at E1. The E2 time-series indicates decoupling of *Pseudo-nitzschia* spp. and pDA that began during the 12–15 October wind reversal (Fig. 4d–g). Detection of elevated pDA in the absence of molecular detection of toxigenic diatoms occurred once, on 21 October at E2 (Fig. 4d–g). This has been observed infrequently in previous experiments (Doucette et al., 2009; Ryan et al., 2011) and may be attributable to the brief (2–3 h) temporal offset between sampling for HAB phytoplankton and sampling for DA quantification.

HAB community variation was clearly related to environmental conditions, however, the nature and degree of significant relationships differed between the two sites (Fig. 4; Table 2). At E1, *Pseudo-nitzschia* spp. abundances were significantly correlated with temperature (inversely) and chlorophyll, while pDA was significantly correlated with temperature and salinity. However, *Alexandrium* and *Heterosigma* exhibited no significant correlations with any environmental parameter. In contrast, at E2 all HAB phytoplankton were significantly correlated with environmental parameters, more consistently and to a higher degree. *Pseudo-nitzschia* abundance showed the highest correlations with salinity (r as high as 0.96), and unlike at E1, *P. australis* and pDA were significantly correlated with beam attenuation (proxy for turbidity). In summary, there was stronger covariation of environmental variation and HAB molecular signals at E2, the site more exposed to direct influence of upwelling filaments.

Table 1
Intra-site correlations for ESP molecular detection results. The upper right bisection represents E1; the lower left bisection represents E2. Molecular marker identifications—auD1: *Pseudo-nitzschia australis*, muD2: *Pseudo-nitzschia multiseries* and/or *P. pseudodelicatissima*, muD1: *Pseudo-nitzschia multiseries*, pDA: particulate domoic acid, Het: *Heterosigma akashiwo*, NA1: *Alexandrium catenella*.

	auD1	muD2	muD1	pDA	Het	NA1
auD1		0.86*		0.82*	−0.01	0.02
muD2	0.93*			0.81*	−0.22	−0.18
muD1	0.97*	0.95*				
pDA	0.47	0.37	0.39		−0.25	−0.19
Het	0.42	0.35	0.42	0.41		0.99*
NA1	0.41	0.31	0.40	0.32	0.95*	

* Correlation is significant at $p < 0.05$.

Table 2
Correlations between ESP molecular detection time-series and environmental variables measured during corresponding periods of sample intake (Fig. 4). Molecular marker identifications are as in Table 1; beam-c is transmissometer beam attenuation. E1 had no detections by probe muD1.

	Temperature	Salinity	Chlorophyll	beam-c
E1				
auD1	−0.57*	0.38	0.48	0.29
muD2	−0.57*	0.43	0.54*	0.37
muD1				
pDA	−0.67*	0.71*	0.40	0.22
Het	−0.02	−0.20	−0.36	0.03
NA1	−0.07	−0.18	−0.30	0.13
E2				
auD1	−0.85*	0.93*	0.79*	0.60*
muD2	−0.83*	0.90*	0.67*	0.49
muD1	−0.85*	0.96*	0.72*	0.49
pDA	−0.61*	0.59*	0.59*	0.69*
Het	−0.67*	0.79*	0.36	0.16
NA1	−0.65*	0.69*	0.33	0.08

* Correlation is significant at $p < 0.05$.

3.3. Transitions in the HAB phytoplankton community

The wind reversal that began on 12 October was stronger and more persistent than the preceding one (Fig. 3a,b), and it resulted in the greatest warming observed at M1 during the experiment (Fig. 3e,g). This event was also associated with the first major transition in the HAB phytoplankton community at E1. Following a period of nearly steady levels, the signal of *Pseudo-nitzschia* and pDA at E1 disappeared between 11 and 15 October (Fig. 4d–f). No marked decreases in chlorophyll concentrations were observed during this transition, however, diurnal variations in chlorophyll became more regular and pronounced during 13–16 October (Fig. 4c). Peak levels in the diurnal chlorophyll variation were consistently observed between ~9 pm and 2 am. These regular variations in ESP chlorophyll measurements were associated with the diurnal vertical migration (across isopycnals) of highly concentrated phytoplankton thin layers, which intersected the moored ESP during the nighttime (Figs. 5a, b). This transition involved a change in the chlorophyll profile from relatively high background with moderately elevated signal of vertically migratory thin layers to relatively low background with highly elevated signal of vertically migratory thin layers (Fig. 5a). Intensification of these layers during 13–15 October coincided with warming of the upper 10 m of the water column (Figs. 5a, c) but with little change in the salinity profile (Fig. 5d). Thus observed changes in density stratification were thermally driven. Average density stratification of the water column at E1 increased by a factor of 3 between 11 and 13 October, and it remained elevated through 15 October.

The presence of dinoflagellate populations around E1, indicated by vertically migratory phytoplankton (Fig. 5), was supported by observations from satellite remote sensing and targeted in situ sampling. Intensely concentrated dinoflagellate bloom patches, evident in visible and near-infrared (NIR) remote sensing, were only observed in the northern bay, where the experiment was focused (Fig. 6). These patchy blooms are evident as enhanced NIR

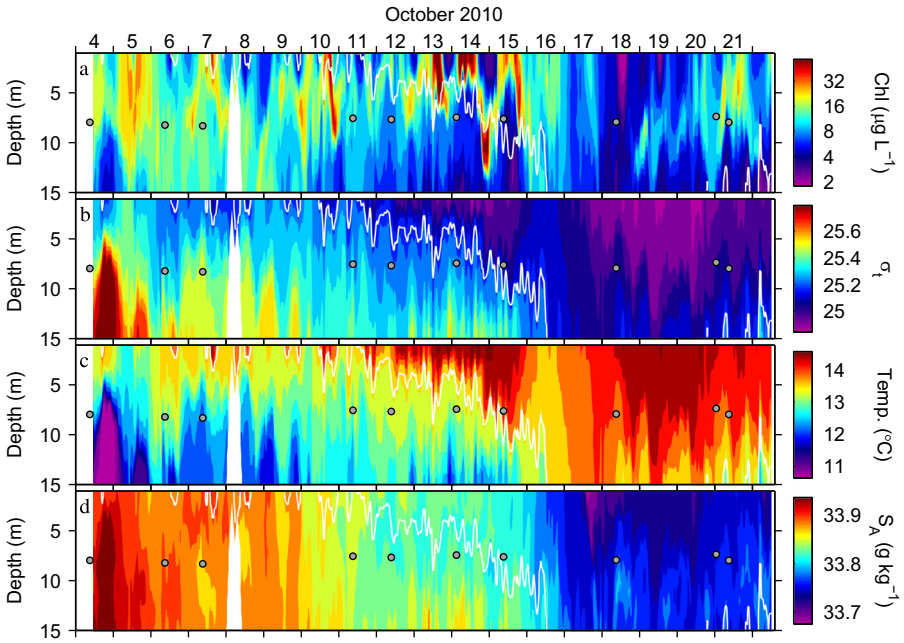

Fig. 5. Water column variability observed 150 m due west of E1. The 25.2 isopycnal is overlaid in all panels (white contour) to illustrate (1) the apparent diurnal vertical migration of phytoplankton across isopycnals and (2) the dominance of temperature variation in determining water density. ESP sample times and depths are indicated by the gray circles. Temporal resolution of profiles is 30 min. Time is PDT. The brief period on 8 October when full water column data are missing was caused by incomplete descent of the profiler.

signal quantified by MERIS MCI, and as reddish features in true-color images (insets of Fig. 6c). E1 was more exposed to dinoflagellate bloom patches than was E2. On 6 October, bloom patches were detected by MERIS only near the coastal boundary (Fig. 6a). A surface bloom filament was then observed extending from near-coastal water to the area south of E1 on 7 October (Fig. 6b).

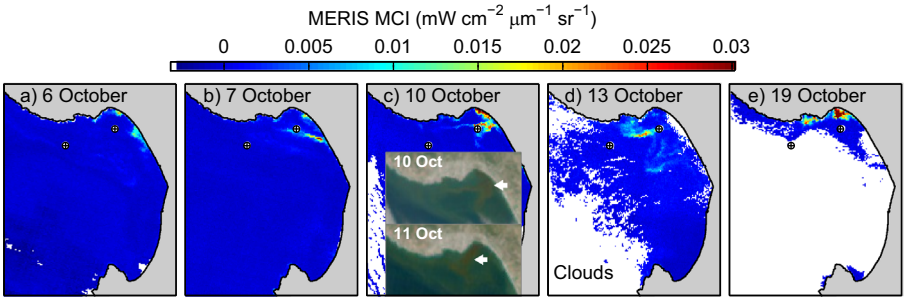

Fig. 6. Near-surface variability of dense dinoflagellate populations. The Maximum chlorophyll index (MCI) from the Medium Resolution Imaging Spectrometer (MERIS) satellite sensor quantifies the near-infrared reflectance signal of intensely concentrated dinoflagellate populations. Insets for the 10 October MCI image (c) are MODIS true color images for 10 and 11 October. The MCI image for this day covered the bay, and the MODIS image insets do not obscure any bloom signal.

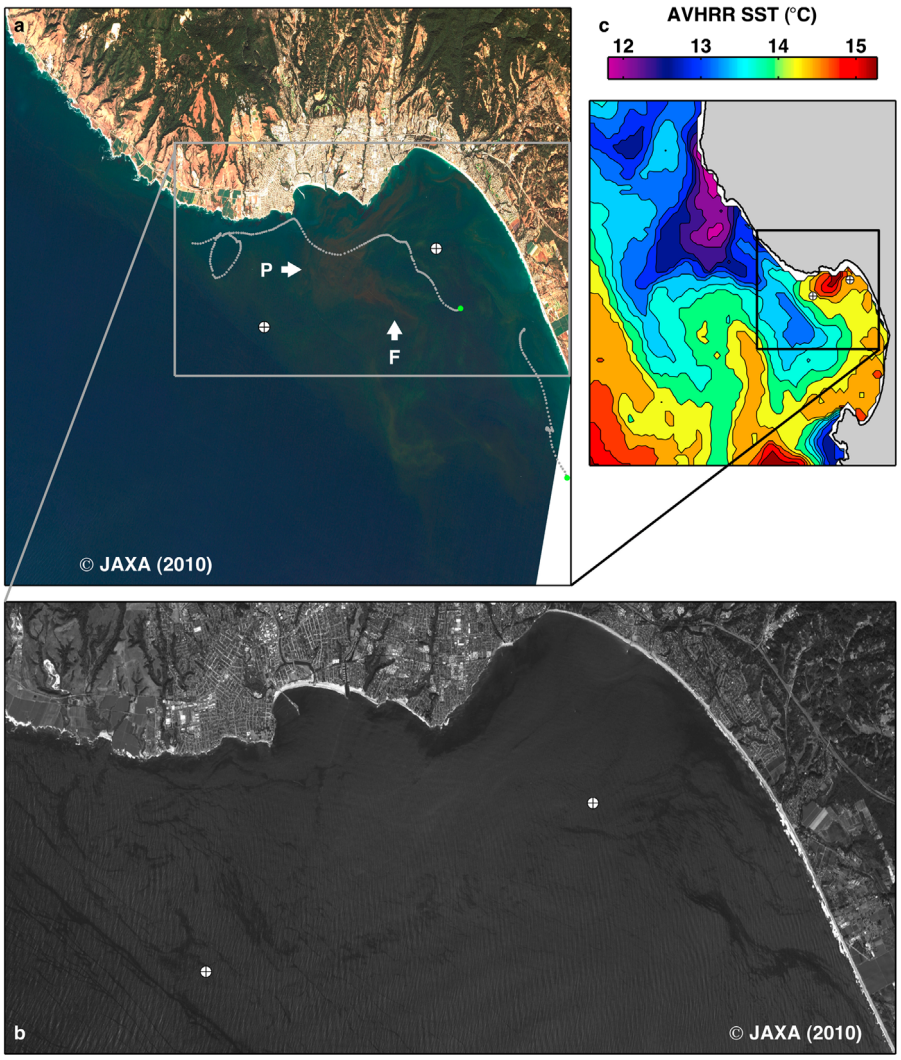

Fig. 7. Patterns and processes of a transition. All images are from 12 October 2010. The color image (a) was derived from 10-m resolution data from the Advanced Visible and Near-Infrared Radiometer, type 2 (AVNIR-2) satellite sensor. The locations of the ESP moorings are indicated, as in Fig. 1. The gray lines show the tracks of drifters, drogued at 3-m depth, illustrating cyclonic surface circulation. Only tracks within the period of 10–12 October are shown; a shorter period is represented for the more southern drifter. Starting points for the drift time-series are indicated by the green dots. Labels P and F indicate a dinoflagellate bloom patch and associated filament. (b) Nadir-viewing image from the Panchromatic Remote-sensing Instrument for Stereo Mapping (PRISM), acquired concurrently with the color image shown in (a). Image resolution is reduced from the original 2.5 m to ~20 m. Black areas in the PRISM image indicate probable convergence zones, which can influence plankton patchiness. (c) Sea surface temperature (SST) from the Advanced Very High Resolution Radiometer (AVHRR). Image times are 03:26 PDT for AVHRR and 14:00 PDT for the AVNIR-2 and PRISM images. (For interpretation of the references to color in this figure caption, the reader is referred to the web version of this article.)

Dinoflagellate bloom signal intensified between 7 and 10 October, and elevated MCI nearly surrounded E1 by 10 October (Figs. 6b, c). The distribution of the bloom patch observed by MERIS on 10 October was described similarly by the MODIS true-color image (Fig. 6c, top inset), confirming the pattern. MODIS data further showed that between 10 and 11 October, the largest bloom patch was advected westward across E1 (Fig. 6c arrows in both insets). After being undetected at E1 on 6 and 7 October, *H. akashiwo* and *A. catenella* were detected consistently starting from 11 October (Fig. 4h,i). By 13 October, the strongest MCI signal was observed immediately west of E1, with indications that the dinoflagellate patch had also been advected and mixed northward and southward (Fig. 6d).

Although the MERIS and MODIS satellite sensors did not acquire clear observations of Monterey Bay between 11 and 13 October, multidisciplinary remote sensing from three other satellite sensors captured transitional conditions on 12 October (Fig. 7). The advecting dinoflagellate bloom patch observed on 10–11 October (Fig. 6c) was observed on 12 October by AVNIR-2 (P in Fig. 7a). Drifter tracks for 10–12 October define a cyclonic circulation underlying transport of the patch from nearshore water into the greater northern bay (Fig. 7a). A filament of the dinoflagellate bloom extended south of the primary patch and E1 on 12 October (F in Fig. 7a), consistent with its southward spreading observed by MERIS (Figs. 6c, d). The exceptionally high spatial resolution of the color image (10 m) illustrates the tremendous patchiness of the near-surface phytoplankton community, as well as the challenges of studying phytoplankton ecology in complex coastal ecosystems. Simultaneous imaging by PRISM suggests a mosaic of small-scale filamentous convergence zones (Fig. 7b), which would have undoubtedly influenced patchiness in the plankton community (e.g. Ryan et al., 2009, 2010a, 2010c).

SST patterns on 12 October reflected regional circulation that was driving local variability at E1 (Fig. 7c). Cool, recently upwelled water extended from the upwelling center north of the bay, southward across the mouth of the bay, and into the central bay. While cool water intruded into the central bay, the warmest water of the northeastern bay extended seaward toward the upwelling filament. These SST patterns are consistent with the cyclonic flow recorded by the drifters and seaward advection of the bloom patch from the northeastern coastal boundary (Figs. 6c, 7a). Enumeration of phytoplankton sampled within the warm bloom patch revealed a population dominated by dinoflagellates, as well as a substantial population of *Pseudo-nitzschia* spp. (Fig. 8). The dominant dinoflagellate, *P. micans*, can cause intense blooms in some regions, resulting in anoxia (Matthews and Pitcher, 1996), but no harmful effects have been reported for this species in Monterey Bay.

Pseudo-nitzschia and pDA signals at E1 both steadily declined and finally disappeared on 15 October, but they returned on 18 October (Fig. 4d–f). Although at lower levels than those detected prior to disappearance, these signals remained at E1 for the remainder of the experiment. Their return followed strongly decreasing salinity and stratification (Fig. 5). Between 15 and 16 October, average density stratification of the water column at E1 decreased by nearly 90%, and it remained low for the remainder of the experiment. Concurrent with the return of *Pseudo-nitzschia*, dinoflagellate bloom populations were evidently concentrated along the northern coastal boundary (Fig. 6e), suggesting the effect of a coastal boundary refuge for certain populations (process 5 in Fig. 2). Although only a limited portion of the bay was visible, this pattern is consistent with known retention of dinoflagellate populations in this area of the bay (Ryan et al., 2008a, 2009).

While *Pseudo-nitzschia* abundance declined at E1 during the wind relaxation period of 12–15 October, it remained steady at E2 (Fig. 4e–g). However, this persistence was short-lived, and they disappeared at E2 between 15 and 18 October. Only one instance of *P. multiseries*/*P. pseudodelicatissima* detection occurred during the remainder of the time-series at E2, on 20 October (Fig. 4e–g). Environmental variation associated with this biological transition at E2 was well observed. Between 15 and 17 October, freshening of the water column occurred all around E2 while vertical stratification of temperature and chlorophyll fluorescence decreased (Fig. 9). Rapid salinity decreases were observed at E2 earlier in the time-series, however, they were followed closely by similarly rapid increases, i.e. oscillatory (Figs. 4b, 7–9 and 12–14 October). These patterns are suggestive of recurrent advection of a front across the mooring site during those periods. However, the rapid salinity decrease that occurred late on 15 October resulted in a sustained change (Fig. 4b) that marked the biological transition at E2.

3.4. The hydrographic history of local HAB phytoplankton community transitions

HAB community transitions coincided with transitions in the hydrographic regime at each ESP (Section 3.3). Here we apply model simulations to examine the source water of the local hydrographic transitions at each ESP (Fig. 10). Model results, which assimilate physical data, were consistent with the more localized environmental data collected at each ESP, and they clarify the boundary interactions involved.

The first transition, during 11–15 October at E1, involved disappearance of *Pseudo-nitzschia* spp. and pDA and appearance

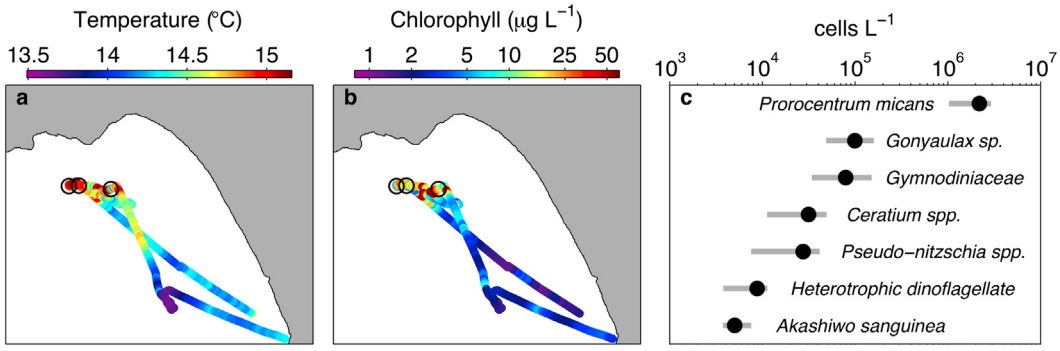

Fig. 8. In situ verification of dinoflagellate bloom advection in warm water of the upwelling shadow. Near-surface (~2 m) measurements of (a) temperature and (b) fluorometric chlorophyll are from 12 October 2010 (Fig. 7). Phytoplankton community composition in the bloom patch (c) shows the range and average for the three sample locations indicated by the black circles in (a) and (b). For these samples, only the most abundant species were enumerated (see Materials and methods).

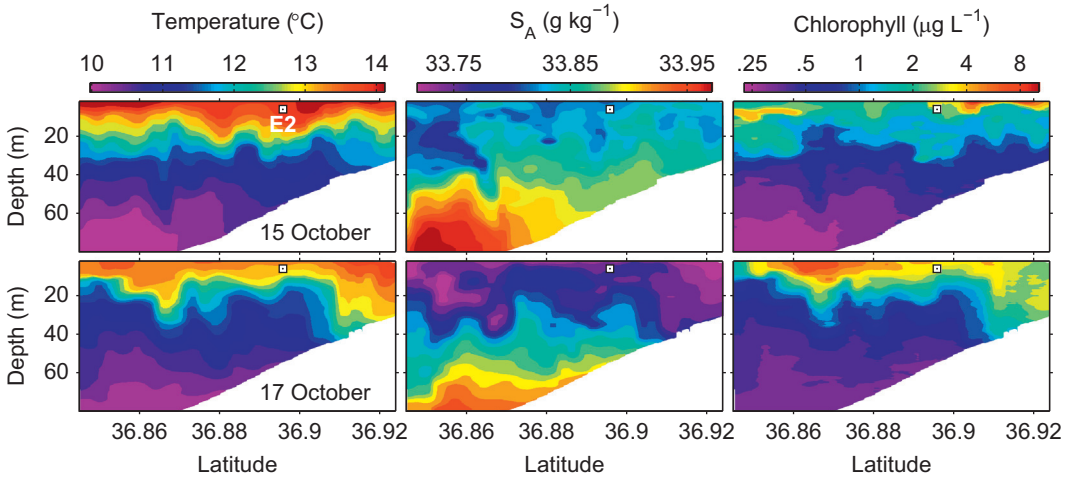

Fig. 9. Water column variability associated with transition of the HAB community at E2 (Fig. 4). The cross-isobath glider sections were parallel to and ~1 km west of the NRL mooring array and E2 (Fig. 1c). The latitude and depth of E2 are marked by a white box symbol in each panel. Each glider sections required ~12 h to complete.

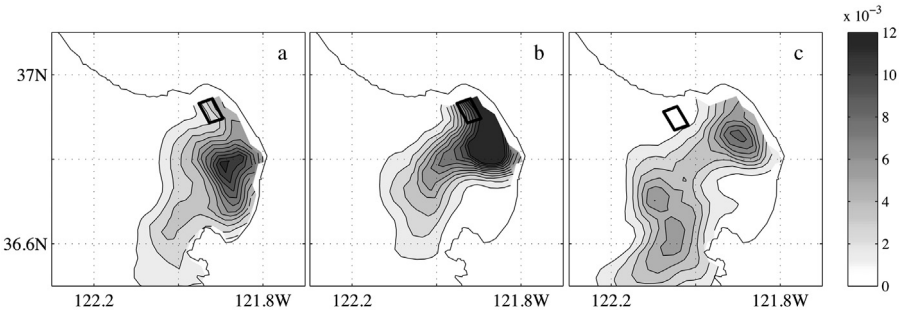

Fig. 10. Tracing source water of ecological transitions at the ESP sites. Results of the adjoint model simulation quantify spatially dependent contributions of tracer-tagged water that was advected and mixed into a volume around an ESP site during the 3.5 days preceding a transition. Simulation seed times define when transitions were apparent in the observations. Transition locations and seed times were (a) E1, 15 October 00:00; (b) E1, 18 October 00:00; and (c) E2, 18 October 00:00.

of *A. catenella* and *H. akashiwo* (Fig. 4), accompanying major changes in stratification and chlorophyll profile structure (Fig. 5). Model results indicate that replacement of water at E1 dominated the transition (Fig. 10a). During this transition in the HAB community, water around E1 was derived mostly from within the bay, south of E1, with some contribution from the area around E1, including the coastal boundary water east of E1. This model result is consistent with the observed cyclonic circulation and dinoflagellate bloom advection from the northern coastal boundary across E1 (Figs. 6, 7).

The second transition, during 15–18 October at E1, involved reappearance of *Pseudo-nitzschia* spp. and pDA (Fig. 4). These changes followed sudden freshening and destratification of the water column, decreased chlorophyll concentrations, and weakening of phytoplankton thin-layer structure (Fig. 5). Model results indicate that during this transition in the HAB community, water around E1 was derived primarily from the northern and central bay (Fig. 10b). In contrast to the previous transition, this indicates a stronger role for local recirculation within the upwelling shadow; a process that may have reintroduced previously flushed populations of *Pseudo-nitzschia* to the area of E1. The simulation also shows a tongue of source water extending into and beyond the mouth of the bay (Fig. 10b), consistent with the freshening observed at E1 in association with this transition (Fig. 5). M1 experienced a steep decrease in salinity during 14–15 October (Fig. 3d), thus making low salinity water accessible to recruitment into inner shelf water during the E1 transition of 15–18 October (Fig. 10b).

The third transition, during 15–18 October at E2, involved disappearance of *Pseudo-nitzschia* and pDA (Fig. 4d–g), accompanying significant hydrographic changes across the entire shelf around E2 (Fig. 9). While the biological changes were similar to the earlier transition observed at E1 during 11–15 October, the hydrographic changes were distinct. In contrast to the relatively constant salinity observed at E1 during the earlier transition, a major decrease in salinity was observed around E2 during 15–18 October. Likewise, model results indicated distinction in the source water supplied to E2 during this later transition. Two primary source regions are indicated: (1) a large region outside the bay and (2) the central northern bay (Fig. 10C). Because offshore water is low in salinity compared to Monterey Bay water and upwelling filaments that enter the bay from the north, supply of water to E2 from the south, seaward of the bay, would explain the decreased salinity associated with this transition (Fig. 9).

3.5. Quasi-Lagrangian study of a Pseudo-nitzschia patch

The importance of understanding biological patchiness is indicated by not only remote sensing observations (Figs. 6, 7), but also by a map of pDA concentrations measured during this experiment (Fig. 11). This map illustrates the wide range of pDA detected in samples from stationary (moorings, pier) and mobile (ship, AUV) sampling platforms. Observations from fixed locations exhibited a great range of variability throughout the experiment, particularly at E1 and SCW. Of all measurements from samples acquired by mobile platforms, the highest pDA concentrations were found in samples acquired toward the southern limit of the

experiment domain (arrow in Fig. 11). Most of these were acquired when two AUVs were deployed to identify, track and sample a phytoplankton patch beginning on 18 October, a transitional time for both E1 and E2 (Section 3.4).

AUV *Dorado* was deployed for large-scale volume surveys on 18–19 and 19–20 October, when it conducted autonomous phytoplankton patch sampling. In both surveys, maximum chlorophyll concentrations were found in the southern survey domain, coincident with the cool side of a front (Fig. 12). Abundant gelatinous zooplankton fouled sensors on *Dorado*, precluding a more comprehensive description of the front. However, sensors on *Tethys* showed increasing salinity and nitrate toward the south (not presented), consistent with a front between the upwelling shadow and recently upwelled water. Phytoplankton enumeration and quantification of pDA from samples acquired by *Dorado* showed that *Pseudo-nitzschia* and pDA were more abundant in the southern high-chlorophyll patch than in patches sampled further north (Fig. 12). Although the abundance of *Pseudo-nitzschia* and pDA generally covaried, there was evidence of anomalously toxic cells. For example, compared to all other samples, sample 2 in the second survey exhibited high toxicity relative to the abundance of toxigenic *Pseudo-nitzschia* (arrow in Fig. 12b).

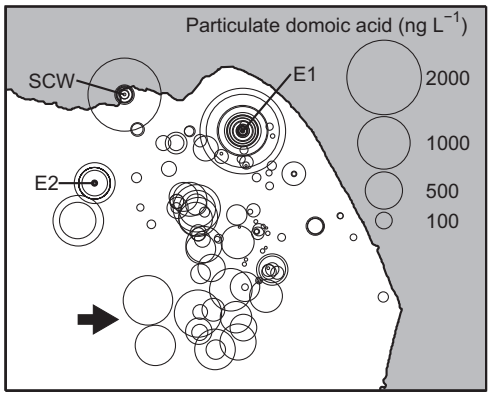

Fig. 11. pDA intensity map based on all sampling during the experiment. Sampling platforms included the two ESPs, the *Dorado* AUV, ship CTD, and a pier off the northern coast. Measurements at fixed locations are labeled: ESP moorings E1 and E2 and the Santa Cruz Wharf (SCW); all other measurements are from analysis of whole-water returned from ship and AUV sampling. Because the pDA assay sensitivity on ESP moorings was exceeded at times (Fig. 4d), signal intensity at these locations is somewhat underestimated in the map. However, ship sampling around E1 supported additional full-range pDA measurements for this location. The arrow indicates the southern extent of AUV-based sampling, where relatively high pDA was sampled using patch localization, tracking and sampling during dual AUV operations (Figs. 12–15).

While AUV *Dorado* applied large-scale volume surveys on prescribed geographic grids, AUV *Tethys* applied algorithms for autonomous vertical and horizontal localization of a phytoplankton patch. On 19 October, *Tethys* localized a phytoplankton-enriched patch in the same area as *Dorado* and began to track it. On 20 October, a drifter was drogued in the patch to serve as a tracking device (Fig. 13a), and *Tethys* began simultaneous drifter (patch) tracking and signal localization. Maximum chlorophyll from each *Tethys* profile was periodically relayed to shore, as a basis for monitoring the patch tracking. The drifter initially moved westward, slowed, then turned southward and accelerated. While tracking the southward flowing patch, *Tethys* was joined by *Dorado*, and dual-AUV mapping and sampling of the patch followed. An animation of this coordinated quasi-Lagrangian tracking is available in the electronic annex of this special issue. Because the patch was moving, reconstruction of chlorophyll patterns in a geographic frame of reference confuses spatial and temporal variation (Fig. 13a). When viewed in the drifter frame of reference, the patch is more clearly distinguished from the lower chlorophyll water surrounding it (Fig. 13b).

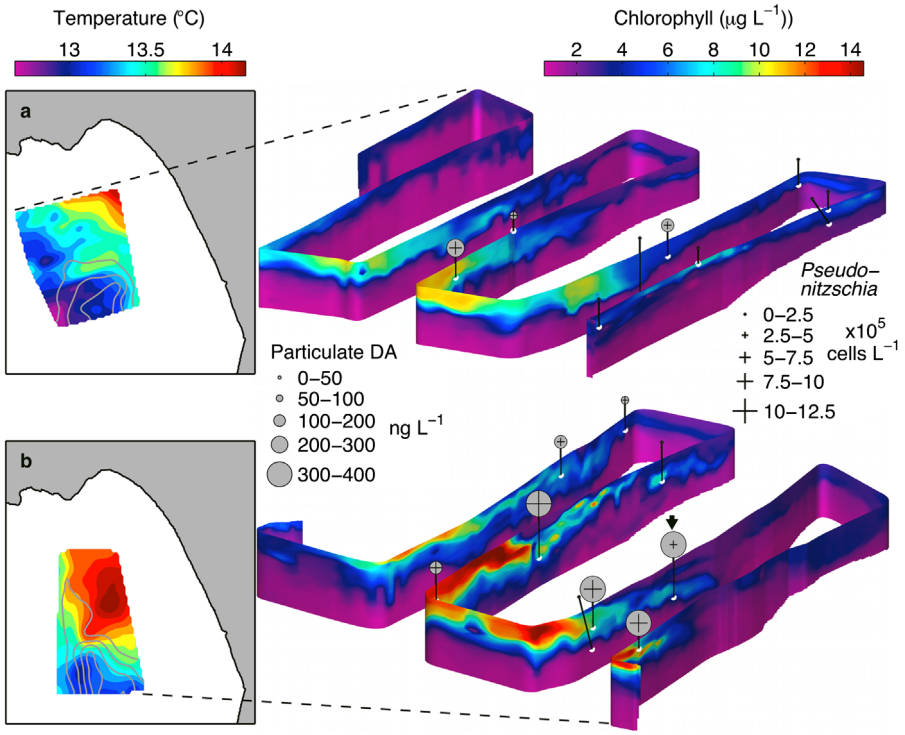

Fig. 12. Patchiness in temperature, chlorophyll, abundance of toxigenic diatoms, and toxin during sequential patch-detection surveys of AUV *Dorado*. Overnight missions were conducted on 18–19 October (a) and 19–20 October (b). The maps show 2–15 m average temperature (color) and chlorophyll (gray contours, 2 μg L^{-1} contour interval at and above 6 μg L^{-1}). Chlorophyll vertical sections (right) are viewed from the SE, above. In both missions, the AUV started from the SE corner. The 4th and 7th samples in (a) and the 4th sample in (b) were control samples targeted at chlorophyll fluorescence signal lower than a statistically defined background level.

Samples from the tracked phytoplankton patch illustrate spatially variable relationships between toxigenic *Pseudo-nitzschia* and pDA, and they suggest the influence of resuspended sediments on toxicity. While *Pseudo-nitzschia* were found in all samples, the highest per-cell toxin levels were found in the first three samples, which were acquired within the first 10 km of the *Dorado* survey (Fig. 14a). These three samples were the only ones acquired from a region in which suspended sediments were coupled with the surface phytoplankton populations (between ~4 and 12 km along transect in Fig. 14a–c). Phytoplankton populations are indicated by the combination of elevated optical backscattering and chlorophyll fluorescence. Sediments are indicated by the combination of elevated optical backscattering and very low chlorophyll fluorescence. A smaller patch of suspended sediments, observed between ~18 and 23.5 km, was evidently not interacting with surface phytoplankton populations. Although the highest concentrations of *Pseudo-nitzschia* were detected outside the zone of sediment – phytoplankton interaction, average per-cell toxicity values were 2.3 times higher within the interaction zone. Fig. 14 shows only the portion of the survey where *Dorado* acquired water samples. The full survey extended over more than twice the distance shown and intersected the sediment – phytoplankton interaction zone two more times.

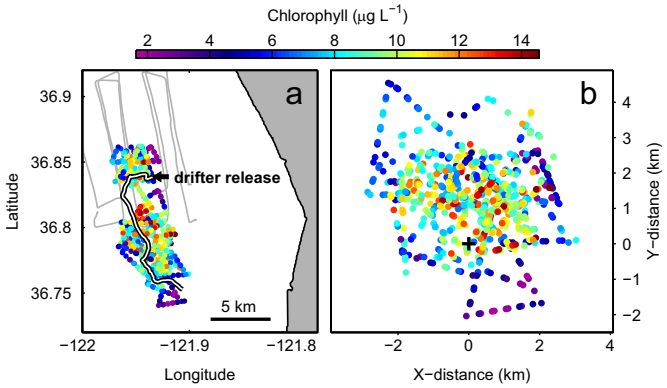

Fig. 13. Lagrangian tracking of a targeted phytoplankton patch. Maps show average chlorophyll in the depth range 2–15 m, in the geographic (a) and drifter (b) frames of reference. The drifter track between 19 October 15:43 and 21 October 14:16 PDT is shown in (a). Dual AUV operations began on 20 October at 15:09 PDT.

Intersecting the suspended sediment patches repeatedly, both AUVs provided data to support a detailed model of the sediment – phytoplankton interaction (Fig. 15). The isosurface illustrates elevated levels of optical backscattering, which were due to phytoplankton at the base of the photosynthetic surface layer, sediments, or both. Interaction between these particle populations is evident where the low-chlorophyll sediment signal of the isosurface extends upward into the higher chlorophyll phytoplankton signal of the isosurface, at the base of the surface phytoplankton layer.

4. Discussion

In a coastal upwelling system, spatial and temporal variations in the direction and magnitude of wind stress largely determine

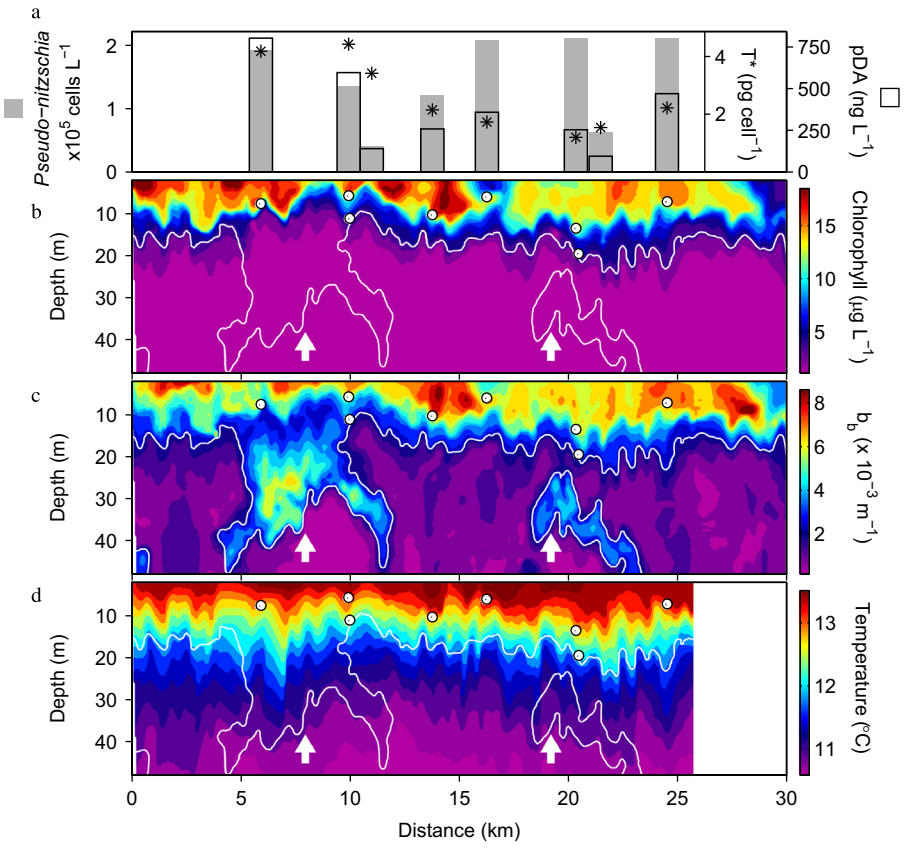

Fig. 14. Relationships between toxigenic diatoms, toxin and water-column processes, from AUV synoptic mapping and water sampling. Abundances of toxigenic *Pseudo-nitzschia* spp. and concentrations of pDA (a) are shown above each AUV sample within the context of water-column conditions (b–d). Sample locations are indicated by the white circles in the vertical sections. Laterally contiguous bars in (a) indicate sample pairs, triggered to sample phytoplankton chlorophyll-peak and off-peak water. T^* in (a) is toxin per-cell. Vertical sections of chlorophyll (b) and optical backscattering at 420 nm (c) illustrate the distribution of phytoplankton and their relationship to suspended sediment patches (arrows). The survey continued an additional 35 km, during which sediment patches were repeatedly encountered and mapped (Fig. 15). However, water samples were not acquired during subsequent encounters because the AUV sample containers were fully utilized within the first 25 km.

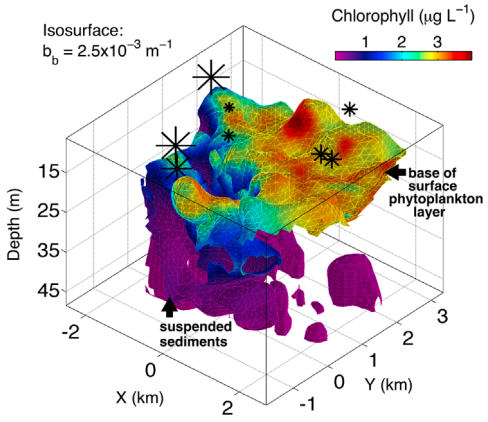

Fig. 15. Quasi-Lagrangian view of the interaction between suspended sediments and the surface phytoplankton layer. The optical backscattering level for the isosurface is the same one used to contour the sediment patches in Fig. 14. This description was derived from intercalibrated measurements by the *Dorado* and *Tethys* AUVs within a 46-h period while following a patch tagged by a satellite-tracked drifter (Fig. 13). X and Y locations are relative to the drifter. At each sample location, toxin per-cell is represented by an asterisk scaled according to the values shown in Fig. 14a.

the response of coastal circulation, mixing, nutrient supply, and stratification (Pitcher et al., 2010). Surface wind stress is thus the primary boundary influence. However, ecosystem structure and function depend greatly upon spatial heterogeneity in wind forcing and its consequences. Existence of the Monterey Bay upwelling shadow is ultimately the result of spatial heterogeneity in atmospheric and oceanic circulation, the patterns of which are determined predominantly by boundary influences of coastal geomorphology: (1) locally weakened surface wind stress caused by mountain-range sheltering, (2) locally reduced and delayed exposure to the flow of upwelling filaments caused by the bay's recess, and (3) locally enhanced residence time caused by the resulting bay circulation patterns (Graham and Largier, 1997). These boundary influences of air–land–sea interaction, in turn, create a dynamic boundary along the outer periphery of the stratification-enhanced upwelling shadow (Ryan et al., 2009, 2010c; Woodson et al., 2009, 2011).

Because Monterey Bay water is a mixture of source water that originates outside the bay, its composition depends on the variable influxes of primary source water types, i.e. water upwelled along the coastal boundary or from Monterey Canyon, and water advected from the dynamic California Current/Undercurrent System (Breaker and Broenkow, 1994; Rosenfeld et al., 1994; Graham and Largier, 1997). Considering the continuously changing hydrography of this open bay, it is reasonable to question whether a seaward boundary can be defined. However, the hydrographic and dynamic distinctions of the upwelling shadow – its locally enhanced stratification and retention – create a dynamic outer boundary that modulates and is modulated by source water influx and bay water outflow (Graham and Largier, 1997; Ryan et al., 2009, 2010a, 2010c; Woodson et al., 2007, 2009, 2011). Such modulated exchange of the upwelling shadow was related to all major transitions in the HAB community observed by the ESP instruments.

The first transition at E1, in which *Pseudo-nitzschia* and pDA disappeared during 11–15 October, was clearly related to the emergence of a distinct type of bloom from the most stratified region of the bay. This emergence was detected by satellite remote sensing, and the underlying cyclonic circulation was defined by drifters. The clear evidence of northeastern bay flushing, advection of a boundary-incubated bloom across E1, and the significant changes in the nature of the chlorophyll profile at E1 indicate that the disappearances of *Pseudo-nitzschia* and pDA were likely due to horizontal displacement of plankton populations. Associated with emergence of the vertically migratory bloom was renewed ESP detection of dinoflagellate and raphidophyte HAB species favored by stratification, *A. catenella* and *H. akashiwo*. Drifters and model simulation results indicate that flow from the southern bay into the northern bay forced seaward flushing of the northeastern bay. Thus, the physical and biological conditions that emanated from the northeastern coastal boundary were evidently part of a cascade of boundary influences that included influx across the southern boundary of the upwelling shadow and flushing of coastal boundary water of the northeastern bay. Tracing the cascade of boundary influences back to a specific type of wind forcing is problematic, however, because the bay's hydrographic responses depend upon a variable history of winds acting upon a variable oceanic background state. Oceanic transitions must often be considered in light of multiple, recent upwelling/relaxation cycles (Pitcher et al., 2010).

The role of incubation and retention of dinoflagellate blooms along the northern coastal boundary of Monterey Bay has been indicated in previous studies (Ryan et al., 2005b, 2008a, 2009; Rienecker et al., 2008). Entrainment of these boundary blooms can initiate larger-scale blooms in the bay, which may subsequently be exported along the coast or dispersed into the boundary current system (Ryan et al., 2008b, 2009; Woodson et al., 2009). Transport of bloom populations back to the coastal boundary can provide a refuge from flushing. The present study indicated the importance of both seeding and retention of coastal-boundary blooms. This apparently consistent pattern in Monterey Bay contrasts with descriptions of dinoflagellate bloom refugia off South Africa, where dinoflagellate populations may incubate in offshore fronts and seed blooms in nearshore water when transported shoreward during relaxation of upwelling (Pitcher et al., 1998, 2010). Bloom refugia may also develop in subsurface phytoplankton thin layers (e.g. McManus et al., 2008) and in the bottom boundary layer (e.g. Welborn, 2000). The role of phytoplankton refugia is an important area of further study for understanding and predicting HABs.

The second transition at E1, in which *Pseudo-nitzschia* and pDA returned between 15 and 18 October, also coincided with multiple boundary influences. These boundary influences are indicated by the coincident decreases in salinity and stratification. Whereas salinity remained relatively constant during the first transition at E1, it dropped sharply throughout the water column during the second transition. This hydrographic change represents the influx of offshore water, which is relatively low in salinity. This low-salinity pulse was evident 1–2 days earlier in the outer bay, at M1, during the wind relaxation/reversal of October 12–15. Its propagation into the inner bay around E1 occurred during a period of upwelling favorable wind forcing, which tends to create a cyclonic flow in the northern bay, and cyclonic flow was observed in HF radar surface currents and drifter tracks during this period (not presented). This illustrates how local responses must often be understood relative to sequences of forcing and response. Whereas the first transition at E1 involved appearance of one phytoplankton ecotype and disappearance of the other, this second transition resulted in their coexistence. The model simulations indicated that the source water of this later transition was mostly from within the northern and central bay, consistent with a cyclonic recirculation that entrained low-salinity water that had previously entered the outer bay. Mixing of the water types present – predominantly Monterey Bay water and water of California Current origin – would have occurred in this circulation, consistent with the observed decrease in salinity at E1. Mixing of the resident *Pseudo-nitzschia* populations and the advecting dinoflagellate bloom would explain the coexistence of ecotypes following this transition. Vertical mixing in outer

bay water would likely have resulted from the enhanced wind stress of this transition, and relatively unstratified conditions, as observed, would have advected inshore to E1 with the cyclonic flow.

The transition at E2 was similar to the first transition at E1 that occurred a few days earlier, in that *Pseudo-nitzschia* disappeared. However, the hydrographic changes accompanying this biological transition were significantly different. Whereas the earlier disappearance of *Pseudo-nitzschia* at E1 involved influx of southern bay water and no significant changes in salinity, the later transition at E2 involved a major influx of offshore water across the seaward boundary of the upwelling shadow and an associated large decrease in salinity.

While the environmental/molecular time-series at fixed locations provided significant insight into local variations in HAB ecology, interpretation of their time-series within the greater context afforded by an ocean observing and modeling system emphasized the importance of understanding patchiness and studying HAB populations in their moving frame of reference. This was a clear lesson from previous ESP network experiments (Ryan et al., 2011). Viewing chlorophyll distributions in the geographic versus patch frames of reference showed how the novel methods developed for AUVs permitted effective localization and tracking of patch bio-optical signal, and hence effective observation in the planktonic frame of reference. This autonomous localization and tracking supported high-resolution mapping of the advecting patch and intelligently targeted sampling within it. These unique observations indicated the potential importance of another boundary influence on HAB ecology. *Pseudo-nitzschia* spp. were present throughout the patch, however, they were distinctly more toxic in an area where they were interacting with resuspended sediments. These results are consistent with results from a previous ESP network study, in which higher pDA levels and greater ($5\times$) variability were measured at the site where resuspended sediments interacted with the phytoplankton, even though *Pseudo-nitzschia* abundances were similar at the two sites (Ryan et al., 2011). Although the exact origin of the suspended particulate matter (SPM) was not observed within the limited domain of the patch-centric sampling in the present study, rain-forced land flushing was not indicated. It is probable that the SPM originated from the shelf bottom boundary layer and was transported into the water column as an intermediate nepheloid layer (INL). INLs are frequently observed in Monterey Bay region, where their significance to phytoplankton (Ryan et al., 2005a, 2011) and zooplankton (Ryan et al., 2010b) ecology is becoming evident. One hypothesis for the observed relationship between resuspended sediments and toxicity is regulation of DA production by trace metals transported with the bottom boundary layer. Laboratory studies have shown that DA production by *Pseudo-nitzschia* is influenced by trace metals (Rue and Bruland, 2001; Maldonado et al., 2002; Rhodes et al., 2006), and resuspended sediments can contain enhanced concentrations of trace metals (e.g. Johnson et al., 1999). An alternative hypothesis is that anomalously toxic *Pseudo-nitzschia* populations were transported from shelf benthic habitat (e.g. Welborn, 2000).

The phytoplankton-enriched patch isolated for Lagrangian studies was located along a front between the relatively warm upwelling shadow water and cooler, presumably more recently upwelled water. Process studies using high-resolution multidisciplinary observations illustrate how the frontal boundary between recently upwelled water and the upwelling shadow functions as a dynamic confluence and mixer of new nutrients and phytoplankton populations (Ryan et al., 2009, 2010c). Further, frontal dynamics are likely to 'spawn' patches, such as the one we tracked. In addition to the boundary influences that crossed the upwelling shadow frontal boundary, the front itself can have important influences on the plankton community. Studies have consistently observed that the seaward boundary of the upwelling shadow typically coincides with an abrupt change in water temperature and color, increased zooplankton biomass and activity at higher trophic levels, surface slicks, and accumulation of buoyant macroalgae and foam that can mark convergence zones (Graham et al., 1992; Graham and Largier, 1997; Woodson et al., 2007). Wind forcing of the buoyant upwelling shadow results in generation of internal waves along its northern frontal boundary, and these waves propagate alongshore and into Monterey Bay, affecting plankton ecology (Woodson et al., 2011). Multidisciplinary remote sensing and in situ observations of the upwelling shadow front indicate that its narrow surface slicks are generated by convergence (and associated accumulation of buoyant surfactants) rather than lateral shear, and that strong cross-frontal mixing can occur beneath the surface convergence (Ryan et al., 2010c). Such observations have also revealed frontal aggregation of phytoplankton and zooplankton, and formation of phytoplankton thin layers by shear and vertical migration (Ryan et al., 2008b, 2010a; Harvey et al., 2012). Interactions between the bottom boundary layer and surface phytoplankton populations have previously been observed on the northern and southern shelf of Monterey Bay, and in both cases the coupling occurred in frontal zones (Ryan et al., 2005a, 2011). Fronts are important loci of ecosystem structure and function.

5. Conclusions

To develop foundational understanding of HAB ecology, upon which predictive models can be based, GEOHAB espouses the integrated application of diverse techniques to discern physical, chemical and biological factors, and their interactions (GEOHAB, 2008). Toward this goal, the observational and modeling system applied in the present study was intended to provide multi-scale, multidisciplinary information to detect processes and define their influence. Within the results, we find that boundary influences at multiple scales manifested as primary influences on HAB phytoplankton populations. The comparative approach espoused by GEOHAB aims to understand HABs through the study of the causative organisms and affected systems in relation to comparable species and systems. Stratification-enhanced upwelling shadows that act as "bloom incubators" are evidently present in all major coastal upwelling ecosystems (e.g. Kahru et al., 2004; Moita et al., 2006; Pitcher and Nelson, 2006; Fawcett et al., 2007; Ryan et al., 2008a). Application of the comparative approach employing integrated observations and modeling across these systems, to better understand the functioning of and interactions between boundary influences, is encouraged.

Acknowledgments

This work was supported by the David and Lucile Packard Foundation, the Naval Research Laboratory (NRL) project "Bio-optical studies of predictability and assimilation in the coastal environment (BIOSPACE), and the National Science Foundation-funded "Lateral mixing and dispersion on the inner shelf " (LatMix) program (Award 0925916 MAM). We thank the MBARI ESP team for the development, preparation and deployment of the ESP instruments and probe arrays: C. Scholin, J. Birch, C. Preston, E. Demir-Hilton, N. Alvarado, B. Roman, S. Jensen, and D. Pargett. The work of J. Harvey was supported by the lab of R. Vrijenhoek. *Tethys* AUV operations were supported by T. Hoover, B. Hobson, and B. Kieft. *Dorado* AUV operations were supported by

H. Thomas, D. Conlin, D. Thompson and the crew of the *R/V Zephyr*, and *Dorado* data processing was supported by M. McCann. We thank B. Teague and H. Wijesekera for providing glider data. I.S. thanks P. Sakalaukus and S. Anderson for assistance with modeling and data analysis. J. Lewis assisted in the extraction of pDA samples. J. Sevadjian provided the SeaHorse profiler data. Drifter operations and ship-based mapping were supported by C. Wahl, M. Blum, G. Friederich, and L. Beatman. Experiment planning and execution were aided by members of the Ocean Decision Support System (ODSS) team: J. Das, T. Maughan, M. McCann, and R. Graham. K. Fulton-Bennett assisted with preparation of Fig. 2.

NOAA Disclaimer: This publication does not constitute an endorsement of any commercial product or intend to be an opinion beyond scientific or other results obtained by the National Oceanic and Atmospheric Administration (NOAA). No reference shall be made to NOAA, or this publication furnished by NOAA, to any advertising or sales promotion that would indicate or imply that NOAA recommends or endorses any proprietary product mentioned herein, or which has as its purpose an interest to cause the advertised product to be used or purchased because of this publication.

Appendix A. Supplementary information

Supplementary data associated with this article can be found in the online version at http://dx.doi.org/10.1016/j.dsr2.2013.01.017.

References

Bellingham, J.G., Streitlien, K., Overland, J., Rajan, S., Stein, P., Stannard, J., Kirkwood, W., Yoerger, D., 2000. An Arctic basin observational capability using AUVs. Oceanography 13, 64–71.

Bellingham, J.G., Zhang, Y., Kerwin, J.E., Erikson, J., Hobson, B., Kieft, B., Godin, M., McEwen, R., Hoover, T., Paul, J., Hamilton, A., Franklin, J., Banka, A., 2010. Efficient propulsion for the Tethys long-range autonomous underwater vehicle. In: Proceedings of IEEE AUV 2010 Monterey, CA, September 2010, pp. 1–6.

Bird, L.E., Sherman, A.D., Ryan, J.P., 2007. Development of an active, large volume, discrete seawater sampler for autonomous underwater vehicles, Proceedings of the Oceans MTS/IEEE, Vancouver, Canada, pp. 1–5.

Bravo, I., Fraga., S., Figueroa, R.I., Pazos, Y., Massanet, A., Ramilo, I., 2010. Bloom dynamics and life cycle strategies of two toxic dinoflagellates in a coastal upwelling system (NW Iberian Peninsula). Deep-Sea Res. II 57, 222–234, http://dx.doi.org/10.1016/j.dsr2.2009.09.004.

Breaker, L.C., Broenkow, W.W., 1994. The circulation of Monterey Bay and related processes. Oceanogr. Mar. Biol.: Annu. Rev. 32, 1–64.

Cazenave, F., Zhang, Y., McPhee-Shaw, E., Bellingham, J.G., Stanton, T.P., 2011. High-resolution surveys of internal tidal waves in Monterey Bay, California, using an autonomous underwater vehicle. Limnol. Oceanogr.: Methods 9, 571–581, http://dx.doi.org/10.4319/lom.2011.9.571.

Cullen, J.J., Eppley, R.W., 1981. Chlorophyll maximum layers of the Southern California Bight and possible mechanisms of their formation and maintenance. Oceanol. Acta 4, 23–32.

Curtiss, C.C., Langlois, G.W., Busse, L.B., Mazzillo, F., Silver, M.W., 2008. The emergence of *Cochlodinium* along the California Coast (USA). Harmful Algae 7, 337–346.

Das, J., Py, F., Maughan, T., O'Reilly, T., Messie, M., Ryan, J., Sukhatme, G., Rajan, K., 2012. Coordinated sampling of dynamic oceanographic features with underwater vehicles and drifters. Int. J. Robot. Res. 31, 626–646, http://dx.doi.org/10.1177/0278364912440736.

Doucette, G.J., Mikulski, C.M., Jones, K.L., King, K.L., Greenfield, D.I., Marin III, R., Jensen, S., Elliott, C.T., Scholin, C.A., 2009. Remote, subsurface detection of the algal toxin domoic acid onboard the environmental sample processor: assay development and field trials. Harmful Algae 8, 880–888.

Doyle, J.D., Jiang, Q., Chao, Y., Farrara, J., 2009. Highresolution real-time modeling of the marine atmospheric boundary layer in support of the AOSNII field campaign. Deep Sea Res. Part II 56, 87–99.

Fawcett, A., Pitcher, G., Bernard, S., Cembella, A., Kudela, R., 2007. Contrasting wind patterns and toxigenic phytoplankton in the southern Benguela upwelling system. Mar. Ecol. Prog. Ser. 348, 19–31.

Fitzwater, S.E., Johnson, K.S., Elrod, V.A., Ryan, J.P., Coletti, L.J., Tanner, S.J., Gordon, R.M., Chavez, F.P., 2003. Iron, nutrient and phytoplankton biomass relationships in upwelled waters of the California coastal system. Cont Shelf Res. 23, 1523–1544.

GEOHAB, 2008. In: Gentien, P., Reguera, B., Yamazaki, H., Fernand, L., Berdalet, E., Raine, R. (Eds.), Global Ecology and Oceanography of Harmful Algal Blooms, GEOHAB Core Research Project: HABs in Stratified Systems. IOC and SCOR, Paris, France, and Newark, Delaware, USA, pp. 59.

Godin, M., Zhang, Y., Ryan, J.P., Hoover, T., Bellingham, J.G., 2011. Phytoplankton bloom patch center localization by the Tethys autonomous underwater vehicle. In: Proceedings of the MTS/IEEE Oceans'11, Kona, HI, USA, September 2011, pp.1–6.

Gower, J., King, S., Borstad, G., Brown, L., 2005. Detection of intense plankton blooms using the 709 nm band of the MERIS imaging spectrometer. Int. J. Remote Sensing 26, 2005–2012.

Graham, W.M., Field, J.G., Potts, D.C., 1992. Persistent 'upwelling shadows' and their influence on zooplankton distributions. Mar.Biol. 114, 561–570.

Graham, W.M., Largier, J.L., 1997. Upwelling shadows as nearshore retention sites: the example of northern Monterey Bay. Cont. Shelf Res. 17, 509–532.

Greenfield, D.I., Marin III, R., Doucette, G.J., Mikulski, C.M., Jones, K.L., Jensen, S., Roman, B., Alvarado, N., Feldman, J., Scholin, C.A., 2008. Field applications of the second-generation environmental sample processor (ESP) for remote detection of harmful algae: 2006–2007. Limnol. Oceanogr.: Methods 6, 667–679.

Harvey, J.B.J., Ryan, J.P., Marin III, R., Preston, C.M., Alvarado, N., Scholin, C.A., Vrijenhoek, R.C., 2012. Robotic sampling, in situ monitoring and molecular detection of marine zooplankton. J. Exp. Mar. Biol. Ecol. 413, 60–70.

Holm-Hansen, O., Amos, A.F., Hewes, C.D., 2000. Reliability of estimating chlorophyll a concentrations in Antarctic waters by measurement of in situ chlorophyll a fluorescence. Mar. Ecol. Prog. Ser. 196, 103–110.

Howard, M., Ladizinsky, N., Cochlan, W., Kudela, R., 2007. Nitrogenous preference of toxigenic Pseudo-nitzschia australis (Bacillariophyceae) from field and laboratory experiments. Harmful Algae 6, 206–217.

IOC, SCOR, IAPSO, 2010. The International Thermodynamic Equation of Seawater – 2010: Calculation and Use of Thermodynamic Properties. Intergovernmental Oceanographic Commission, Manuals and Guides No. 56, UNESCO (English), 196 pp.

Jessup, D.A., Miller, M.A., Ryan, J.P., Nevins, H.M., Kerkering, H.A., Mekebri, A., Crane, D.B., Johnson, T.A., Kudela, R.M., 2009. Mass stranding of marine birds caused by a surfactant-producing red tide. PLoS ONE 4, e4550, http://dx.doi.org/10.1371/journal.pone.0004550.

Johnson, K.S., Needoba, J.A., 2008. Mapping the spatial variability of plankton metabolism using nitrate and oxygen sensors on an autonomous underwater vehicle. Limnol. Oceanogr. 53, 2237–2250.

Johnson, K.S., Chavez, F.P., Friederich, G.E., 1999. Continental-shelf sediment as a primary source of iron for coastal phytoplankton. Nature 398 (6729), 697–700.

Kahru, M., Mitchell, B.G., Diaz, A., Miura, M., 2004. MODIS detects a devastating algal bloom in Paracas Bay, Peru. Eos, Trans. Am. Geophys. Union 85, 465–472.

Klinck, J.M., 1996. Circulation near submarine canyons: a modeling study. J. Geophys. Res. 101, 1211–1223.

Kudela, R., Pitcher, G., Probyn, T., Figueiras, F., Moita, T., Trainer, V., 2005. Harmful algal blooms in coastal upwelling systems. Oceanography 18, 184–197.

Kudela, R.M., Ryan, J.P., Blakely, M.D., Lane, J.Q., Peterson, T.D., 2008a. Linking the physiology and ecology of *Cochlodinium* to better understand harmful algal bloom events: a comparative approach. Harmful Algae 7, 278–292.

Kudela, R., Lane, J., Cochlan, W., 2008b. The potential role of anthropogenically derived nitrogen in the growth of harmful algae in California, USA. Harmful Algae 8, 103–110.

Kudela, R.M., Seeyave, S., Cochlan, W.P., 2010. The role of nutrients in regulation and promotion of harmful algal blooms in upwelling systems. Prog. Oceanogr. 85, 122–135, http://dx.doi.org/10.1016/j.pocean.2010.02.008.

Mackey, K.R.M., Mioni, C.E., Ryan, J.P., Paytan, A., 2012. Phosphorus cycling in the red tide incubator region of Monterey Bay in response to upwelling. Front. Microbiol. 3, 33, http://dx.doi.org/10.3389/fmicb.2012.00033.

Maldonado, M.T., Hughes, M.P., Rue, E.L., Wells, M.L., 2002. The effect of Fe and Cu on growth and domoic acid production by pseudo-nitzschia multiseries and Pseudo-nitzschia australis. Limnol. Oceanogr. 47, 515–526.

Matthews, S.G., Pitcher, G.C., 1996. Worst recorded marine mortality on the South African coast. Harmful and Toxic Algal Blooms. In: International Conference on Marine Toxic Phytoplankton, Sendai (Japan), UNESCO, Paris, p. 89–92.

Mazzillo F.F.M., Ryan J.P.,Silver M.W., 2011 Parasitism as a biological control agent of dino flagellate blooms in the California Current System. Harmful Algae 10(6), 763–773.

McManus, M.A., Kudela, R.M., Silver, M.W., Steward, G.F., Donaghay, P.L., Sullivan, J.M., 2008. Cryptic blooms: are thin layers the missing connection? Estuaries Coasts: J. CERF 31, 396–401, http://dx.doi.org/10.1007/s12237-007-9025-4.

Moita, M.T., Palma, S., Oliviera, P.B., Vidal, T., Silva, A., Vilarinho, M.G., 2006. The return of *Gymnodinium catenatum* after 10 years: bloom initiation and transport of the Portuguese coast. In: Proceedings of 12th International Congress on Harmful Algae, PO.06-14, September 2006, Copenhagen.

O'Halloran, C., Silver, M.W., Holman, T.R., Scholin, C.A., 2006. *Heterosigma akashiwo* in central California waters. Harmful Algae 5, 124–132.

Penta, B., 2011, BIOSPACE/DYABOLIC October 2010 Field Program, Monterey Bay, California, Data Report, NRL/MR/7330—11-9342.

Pitcher, G.C., Boyd, A.J., Horstman, D.A., Mitchell-Innes, B.A., 1998. Subsurface dinoflagellate populations, frontal blooms and the formation of red tide in the southern Benguela upwelling system. Mar. Ecol. Prog. Ser. 172, 253–264.

Pitcher, G.C., Nelson, G., 2006. Characteristics of the surface boundary layer important to the development of red tide on the southern Namaqua shelf of the Benguela upwelling system. Limnol. Oceanogr. 51, 2660–2674.

Pitcher, G.C., Figueiras, F.G., Hickey, B.M., Moita, M.T., 2010. The physical oceanography of upwelling systems and the development of harmful algal blooms. Prog. Oceanogr. 85, 5–32, http://dx.doi.org/10.1016/j.pocean.2010.02.002.

Preston, C.M., Harris, A., Ryan, J.P., Roman, B., Marin III, R., et al., 2011. Underwater application of quantitative PCR on an ocean mooring. PLoS ONE 6 (8), e22522.

Ramp, S.R., Paduan, J.D., Shulman, I., Kindle, J., Bahr, F.L., Chavez, F.P., 2005. Observations of upwelling and relaxation events in the northern Monterey Bay during August 2000. J. Geophys. Res. 110, C07013, http://dx.doi.org/10.1029/2004JC002538.

Rhodes, L., Selwood, A., McNabb, P., Briggs, L., Adamson, J., van Ginkel, R., Laczka, O., 2006. Trace metal effects on the production of biotoxins by microalgae. Afr. J. Mar. Sci. 28, 393–397.

Rienecker, E.R., Ryan, J.P., Marin III, R., Blum, M., Dietz, C., Chavez, F.P., 2008. Synoptic mapping of the phytoplankton size distribution, with applications to the ecology of red tides and harmful algal blooms. Limnol. Oceanogr.: Methods 6, 153–161.

Rosenfeld, L.K., Schwing, F.B., Garfield, N., Tracy, D.E., 1994. Bifurcated flow from an upwelling center: a cold water source for Monterey Bay. Cont. Shelf Res. 14, 931–964.

Rue, E., Bruland, K., 2001. Domoic acid binds iron and copper: a possible role for the toxin produced by the marine diatom Pseudo-nitzschia. Mar. Chem. 76, 127–134.

Ryan, J.P., Chavez, F.P., Bellingham, J.G., 2005a. Physical-biological coupling in Monterey Bay, California: topographic influences on phytoplankton ecology. Mar. Ecol. Prog. Ser. 287, 23–32.

Ryan, J.P., Dierssen, H.M., Kudela, R.M., Scholin, C.A., Johnson, K.S., Sullivan, J.M., Fischer, A.M., Rienecker, E.V., McEnaney, P.R., Chavez, F.P., 2005b. Coastal ocean physics and red tides, an example from Monterey Bay, California. Oceanography 18, 246–255.

Ryan, J.P., Gower, J.F.R., King, S.A., Bissett, W.P., Fischer, A.M., Kudela, R.M., Kolber, Z., Mazzillo, F., Rienecker, E.V., Chavez, F.P., 2008a. A coastal ocean extreme bloom incubator. Geophys. Res. Lett. 35, L12602, http://dx.doi.org/10.1029/2008GL034081.

Ryan, J.P., McManus, M.A., Paduan, J.D., Chavez, F.P., 2008b. Phytoplankton thin layers within coastal upwelling system fronts. Mar. Ecol. Prog. Ser. 354, 21–34.

Ryan, J.P., Fischer, A.M., Kudela, R.M., Gower, J.F.R., King, S.A., Marin III, R., Chavez, F.P., 2009. Influences of upwelling and downwelling winds on red tide bloom dynamics in Monterey Bay, California. Cont. Shelf Res. 29, 785–795.

Ryan, J.P., McManus, M.A., Sullivan, J.M., 2010a. Interacting physical, chemical and biological forcing of phytoplankton thin-layer variability in Monterey Bay, California. Cont. Shelf Res. 30, 7–16.

Ryan, J.P., Johnson, S.B., Sherman, A., Rajan, K., Py, F., Thomas, H., Harvey, J.B.J., Bird, L., Paduan, J.D., Vrijenhoek, R.C., 2010b. Mobile autonomous process sampling within coastal ocean observing systems. Limnol. Oceanogr.: Methods 8, 394–402.

Ryan, J.P., Fischer, A.M., Kudela, R.M., McManus, M.A., Myers, J.S., Paduan, J.D., Ruhsam, C.M., Woodson, C.B., Zhang, Y., 2010c. Recurrent frontal slicks of a coastal ocean upwelling shadow. J. Geophys. Res. 115, C12070, http://dx.doi.org/10.1029/2010JC006398.

Ryan, J., Greenfield, D., MarinIII, R., Preston, C., Roman, B., Jensen, S., Pargett, D., Birch, J., Mikulski, C., Doucette, G., Scholin, C., 2011. Harmful phytoplankton ecology studies using an autonomous molecular analytical and ocean observing network. Limnol. Oceanogr 56 (4), 1255–1272.

Scholin, C.A., Gulland, F., Doucette, G.J., Benson, S., Busman, M., Chavez, F.P., Cordaro, J., DeLong, R., De Vogelaere, A., Harvey, J., Haulena, M., Lefebvre, K., Lipscomb, P.D.R., Loscutoff, S., Lowenstine, L.J., Marin III, R., Miller, P.E., McLellan, W.A., Moeller, P.D.R., Powell, C.L., Rowles, T., Silvagni, P., Silver, M., Spraker, T., Trainer, V., Van Dolah, F.M., 2000. Mortality of sea lions along the central California coast linked to a toxic diatom bloom. Nature 403, 80–84.

Scholin, C., Doucette, G., Jensen, S., Roman, B., Pargett, D., Marin III, R., Preston, C., Jones, W., Feldman, J., Everlove, C., Harris, A., Alvarado, N., Massion, E., Birch, J., Greenfield, D., Vrijenhoek, R., Mikulski, C., Jones, K., 2009. Remote detection of marine microbes, small invertebrates, harmful algae and biotoxins using the Environmental Sample Processor (ESP). Oceanography 22, 158–167.

Shea, R.E., Broenkow, W.W., 1982. The role of internal tides in the nutrient enrichment of Monterey Bay, California. Estuarine Coastal Shelf Sci. 15, 57–66.

Shulman, I., Anderson, S., Rowley, C., deRada, S., Doyle, J., Ramp, S., 2010. Comparisons of upwelling and relaxation events in the Monterey Bay area. J. Geophys. Res. V.115, C06016, http://dx.doi.org/10.1029/2009JC005483.

Shulman, I., Moline, M.A., Penta, B., Anderson, S., Oliver, M., Haddock, S.H.D., 2011. Observed and modeled bio-optical, bioluminescent, and physical properties during a coastal upwelling event in Monterey Bay, California. J. Geophys. Res. 116, C01018, http://dx.doi.org/10.1029/2010JC006525.

Smayda, T.J., 2010. Adaptations and selection of harmful and other dinoflagellate species in upwelling systems. 2. Motility and migratory behaviour. Prog. Oceanogr. 85, 71–91, http://dx.doi.org/10.1016/j.pocean.2010.02.005.

Smayda, T.J., Trainer, V.L., 2010. Dinoflagellate blooms in upwelling systems: seeding, variability, and contrasts with diatom bloom behavior. Prog. Oceanogr. 85, 92–107, http://dx.doi.org/10.1016/j.pocean.2010.02.006.

Trainer, V.L., Adams, N.G., Bill, B.D., Stehr, C.M., Wekell, J.C., Moeller, P., Busman, M., Woodruff, D., 2000. Domoic acid production near California coastal upwelling zones, June 1998. Limnol. Oceanogr. 45, 1818–1833.

Trainer, V.L., Pitcher, G.C., Reguera, B., Smayda, T.J., 2010. The distribution and impacts of harmful algal bloom species in eastern boundary upwelling systems. Prog. Oceanogr. 85, 33–52, http://dx.doi.org/10.1016/j.pocean.2010.02.003.

Wang, Z., Maucher-Fuquay, J., Fire, S.E., Mikulski, C.M., Haynes, B., Doucette, G.J., Ramsdell, J.S., 2012. Optimization of solid-phase extraction and liquid chromatography-tandem mass spectrometry for the determination of domoic acid in seawater, phytoplankton, and mammalian fluids and tissues. Anal. Chim. Acta 715, 71–79.

Welborn, V., 2000. Pseudo-nitzschia in nearshore sediments and entry of domoic acid (DA) into benthic communities, MS Thesis, UC Santa Cruz.

Woodson, C.B., Eerkes-Medrano, D.I., Flores-Morales, A., Foley, M.M., Henkel, S.K., Hessing-Lewis, M., Jacinto, D., Needles, L., Nishizaki, M.T., O'Leary, J., Ostrander, C.E., Pespeni, M., Schwager, K.B., Tyburczy, J.A., Weersing, K.A., Kirincich, A.R., Barth, J.A., McManus, M.A., Washburn, L., 2007. Local diurnal upwelling driven by sea breezes in northern Monterey Bay. Cont. Shelf Res. 27, 2289–2302.

Woodson, C.B., Washburn, L., Barth, J.A., Hoover, D.J., Kirincich, A.R., McManus, M.A., Ryan, J.P., Tyburczy, J., 2009. Northern Monterey Bay upwelling shadow front: Observations of a coastally and surface-trapped buoyant plume. J. Geophys. Res. 114, C12013, http://dx.doi.org/10.1029/2009JC005623.

Woodson, C.B., Barth, J.A., Cheriton, O.M., McManus, M.A., Ryan, J.P., Washburn, L., et al., 2011. Observations of internal wave packets propagating along-shelf in northern Monterey Bay. Geophys. Res. Lett. 38, L01605, http://dx.doi.org/10.1029/2010GL045453.

Zhang, Y., McEwen, R.S., Ryan, J.P., Bellingham, J.G., 2010. Design and tests of an adaptive triggering method for capturing peak samples in a thin phytoplankton layer by an autonomous underwater vehicle. IEEE J. Ocean. Eng. 35, 785–796, http://dx.doi.org/10.1109/JOE.2010.2081031.